Politecnico di Torino

Politecnico di Torino

Corso di Laurea
A.a. 2024/2025
Sessione di Laurea Luglio 2025

Wind Farm Wake Modelling and Layout Optimization using Numerical Tools

Relatori:
Giuseppe Giorgi
Giovanni Bracco
Alberto Ghigo

Candidato:
Lorenzo De Nuccio

ABSTRACT

The thesis addressed the issue of the wakes and their aerodynamical losses generated by wind farm turbines from two main perspectives: the potential microclimatic impacts they may cause in the surrounding environment (particularly if directed towards the mainland in the case of large offshore wind farms) and the degradation in performance and Annual Energy Production (AEP). The proposed methodology involved two software tools, PyWake and FLORIS, developed respectively by DTU and NREL, whose potential applications have been highlighted. These software tools implement a range of different analytical wake models and are capable of simulating wake propagation and assessing the resulting downwind velocity deficits comparing their behaviours. Once a case study has been selected, the potential impacts of the wake propagation have been evaluated: the microclimatic impacts aspect has been tackled by qualitatively and quantitatively comparing the velocity losses caused by wakes for each of the five wake models selected across both software tools. The results highlighted substantial differences between some of the presented models, confirming the need for benchmarking by other tools to validate the correct wake behaviour, but, overall, a limited impact was observed for every simulation. Regarding the optimization aspect, starting from the existing *YawOptimizer* function in FLORIS, a yaw control strategy algorithm has been implemented in PyWake, aimed at finding the optimal yaw angles in terms of energy production on an annual basis, to leverage this strategy with the various wake models within the PyWake library. Specific yaw angles can reduce the wake influence on the performance of downwind turbines, thereby enabling greater overall power extraction and, consequently, higher annual energy production. In this case as well, the improvements have been evaluated based on the selected wake model, yielding different results depending on the typical wake behaviour of each model: while some models have shown excellent results in terms of production increase, demonstrating how wake deficit can be impactful, others do not appear to be very sensitive to yaw control, which is why a benchmark to verify the proper behaviour of the wake is considered necessary.

CONTENTS

LIST OF TABLES AND FIGURES

1. Introduction and thesis outline

Nowadays, climate change and global warming are major issues that must be addressed appropriately. In this context, the transition from fossil fuels to renewable energy sources appears to be the only solution to limit the environmental impact of human activity without reducing the necessary energy supply. Among the renewable energy sources gaining increasing attention in recent studies, there are solar and wind energy; consequently, more and more projects based on these technologies are being developed worldwide. According to the latest IEA report [1], global energy production from renewable sources is expected to grow by 2.7 times by 2030 compared to current levels, with 5,500 GW of new capacity to be added. Specifically, electricity generated from wind resources is expected to double by the same year, reaching around 5,000 TWh/year. This forecasted rapid growth takes into account the large amount of energy that can be extracted from offshore wind power plants, which offer a high capacity factor. This parameter reflects the performance of a resource and is particularly important for renewable sources, which depend on atmospheric phenomena and geomorphological characteristics that vary by location and time, making them less consistent. Offshore wind farms take advantage of the characteristics of sea winds, which are more constant over time and uniform in space due to the absence of obstacles, thus offering great long-term production potential.

In recent years, Europe has become a leader in offshore wind development [2], thanks to a series of measures taken by individual member states (in Italy, decrees such as FER1 and FER2 [3]) aimed at encouraging investments in marine areas morphologically suitable for constructing such facilities, like the Baltic Sea and the North Sea, which have very shallow seabeds. Despite the various challenges that the installation of new plants will face—such as limited port capacity for transporting materials and service equipment, as well as grid limitations on the input power—Europe is expected to reach a total installed offshore capacity of 84 GW by 2030, with Italy ready to contribute, albeit to a limited extent, to this increase [2].

The vast number of projects currently under development has raised concerns about the potential environmental impact that large offshore wind farms might have on their surrounding environment. In particular, attention has been drawn to the turbulence generated by the movement of large air masses downwind of a wind farm, which propagates to create what is known as a “wake”. This wake can

alter the atmospheric boundary layer (ABL) above the sea, potentially causing significant changes in wind speed, humidity, or temperature [4]. This layer extends up to 3 km above the Earth's surface and differs from the rest of the atmosphere above it because it is directly affected by surface-level phenomena, such as solar heating of the surface or changes in the momentum of air caused by obstacles encountered by the wind [5]. Focusing on this last example, large wind turbines act as obstacles that can modify the transfer of momentum between different air masses within the ABL, creating an imbalance whose consequences are not yet fully understood [6][7].

One important process occurring within this boundary layer is the exchange of heat between the ocean and the atmosphere. This process can be described through four key terms: the net upward latent heat flux (LH), the net upward sensible heat flux (SH), the net upward longwave surface radiation (LW), and the net downward shortwave surface radiation (SW). The net upward heat flux (NH) is the algebraic sum of these four components, where the first three are positive and the last one is negative. Among these, the component most affected by the presence of wind farms throughout the year is SH, which tends to decrease (by as much as 4 W/m^2 in some parts of the North Sea), leading to a reduction in NH. This dispersion is particularly significant during winter months, when the heat exchange from the ocean to the overlying air is more intense than during other times of the year. This effect may even lead to a potential reduction in sea surface temperature of up to 0.25 °C [7]. Other possible consequences include the formation of fog or low-level cloud formations, which in turn could influence the amount of precipitation in the area. That said, although current wind farms have, on some days, shown considerable variations in precipitation compared to the average, these variations are generally minor when compared to long-term rainfall variability.

The aim of this thesis is to evaluate the effectiveness of algorithms used to analyse such phenomena. Specifically, two analytically simple tools, PyWake and FLORIS, will be examined. These tools are widely used for preliminary analyses and are capable of achieving good accuracy. Subsequently, the use of a combined approach between the two will be assessed.

2. Bibliography

2.1. Tools

2.1.1. Numerical tools

To examine this type of phenomenon, there are various options that can be considered. Numerical tools are the simplest to implement, because they are "black-box" tools. They follow a semi-empirical approach, modelling a simplified profile of the wakes, not considering data like the geometry of the turbine, and approximating turbulence near the blades. Computational resources needed for this kind of approach are very limited, so the use of numerical tools can be convenient if we need a rapid evaluation of the wake development in a layout. Some examples of software that work in this way are WAsP [8], PyWake [9] and FLORIS [10].

2.1.2. Actuator Disk Model tools

If we look for a more precise analysis, data validation is needed, so numerical tools are not useful anymore, because of their lack of accuracy. In alternative, tools that work with the Actuator Disc Model can be used [11]. The model represents the area swept by the rotor as a porous disk exerting opposite forces with the respect to the incoming flow, extracting a part of its momentum, modifying the velocity field. The calculation of momentum and wind speed losses is carried out by Reynolds-Averaged Navier-Stokes equation (RANS), solved in a finite volume. This kind of approach is more accurate, giving better results in terms of turbulence, and a good representation of the velocity field far from the turbine (far-wake) is produced. Nevertheless, centrifugal forces and vorticity near the rotor is not well modelled, so if we look for detailed profiles of the wake near the turbine (near-wake), the ADM is not the best choice. Tools like PALM [12] and WindSE [13] implement the ADM in their algorithms.

2.1.3. Computational Fluid Dynamics

The most accurate analysis is carried out through Computational Fluid Dynamics (CFD), to define turbulences and how they propagate. CFD tools solve RANS equations, but unlike ADM tools, they implement a more precise model, the Actuator Line Model (ALM) [14], which models the turbine as an actuator line where resistive forces act on the blade profiles, so they influence the surrounding flow. With the choice of a fine mesh, a precise definition of what happen close to

the turbine can be obtained. These types of tools require a very high computational cost, so are used if we need a considerable accuracy, or to validate data obtained from other analysis. In this category, we can mention tools like SOWFA [15] and OpenFOAM [16].

By the way, for a preliminary approach, many numerical tools are considered quite accurate even if compared to CFD instruments. In the following paragraphs, PyWake and FLORIS have been expounded.

2.2. PyWake

PyWake [9] is a Python-based tool that enables detailed analysis of the wake effects generated by wind turbines in a wind farm, in terms of both energy production and velocity field. It is capable of handling multiple input variables simultaneously, thanks to the selection of an engineering model that encapsulates all the characteristics of the wind farm under study. The engineering model is the core of the software; therefore, in order to achieve a detailed analysis in a short time, it must be carefully selected. It consists of a base model for the wind farm, to which a wake model and other secondary models, containing specific features such as turbulence or the overlap of effects, are associated.

2.2.1. Wind Farm Models

There are three wind farm models in PyWake library:

- PropagateDownwind; this is the simplest model; it operates iterations on every turbine, proceeding downstream from the first turbine to the last. The main assumption of this model is that a turbine affects the other ones only downstream, so no turbines can influence the ones in front of them.
- All2AllIterative; this model considers instead the blockage effect of the turbines too: each turbine influences the behaviour of the flux near every other turbine, so the solution has to be found through many iterations, until convergency is reached. Its use is common only in case of very complex layouts, because of its high computational cost.
- PropagateUpDownIterative; this model uses a hybrid strategy between the other two, mixing upwind and downwind calculations. Its computational cost is medium and it's useful when yaw effects need to be examined in detail.

2.2.2. Wake Deficit Models

The next fundamental part in the model building is the choice of the wake model. Many studies have been carried out in the last years, so many wake models have been created, everyone with different characteristics and equations which describe them. The wake model contains in it the process of calculation of wind speed deficit for every part the wake invests. Among the big number of models, we can distinguish two categories:

- Top-Hat models; simple analytical models, which assume the wake with a top-hat shape. They are used for analysing wake effects on a big scale, because of their capability of identifying correctly the intensity of the far-wake. The most important top-hat model, as well as the first wake model ever defined, is the Jensen [17] one, that defines the velocity V in the wake as:

$$V = U\left(1 - 2\alpha\left(\frac{r_o}{r_o + \alpha x}\right)^2\right)$$

  Where U is the free stream velocity, r_o the rotor radius, x the distance from the rotor and α the entrainment constant.

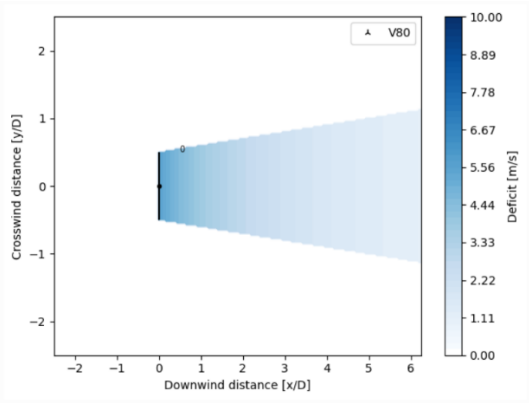

Figure 1: Wake modelling using Jensen model (PyWake)

- Gaussian models: they assume a shorter wake, giving a more accurate representation of the near-wake, and the blockage effects too (Fuga models). The most representative model of this kind is the Bastankhah and Porté-Agel model [18], that assumes a gaussian shaped profile for the wake, and a deficit that is dependent on the thrust coefficient of the turbine, leading to a representation of this kind:

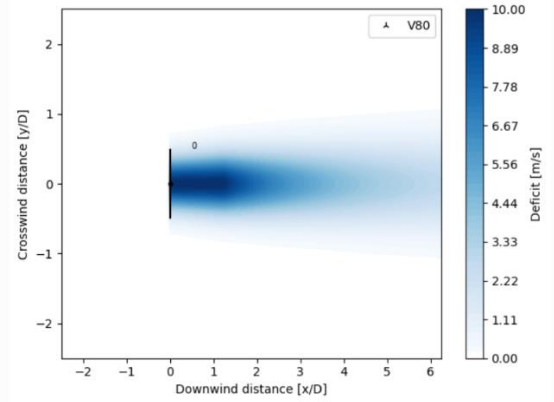

Figure 2: Wake modeling using Bastankhah and Porté-Agel model

A big number of gaussian models has been developed in the last 10 years, to overcome the inability of models like the Bastankhah one to calculate the correct deficit in the far-wake. So now there are many models that achieve a good accuracy for both near and far wake. Among these, we can cite the Zong model (2020) [19] and the SuperGaussian model (2023) [20]:

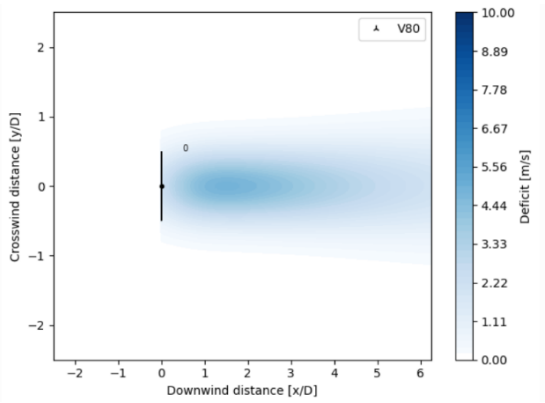

Figure 3: Wake modelling using Zong and Porté-Agel model

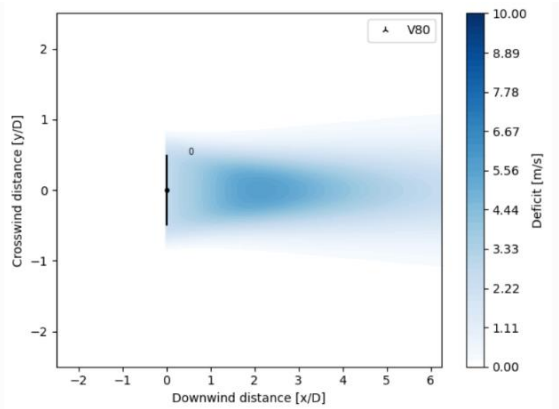

Figure 4: Wake modelling using SuperGaussian model

2.2.3. Additional Models

To complete the modelling, it is essential to include additional information regarding the interactions between the turbines themselves. Among the models that refine the calculation in this regard, the following can be implemented:

- Superposition model: this model defines how the wake effects generated by one turbine are combined with those produced by all the others, in order to describe the interaction among different wakes generated within the wind farm. Different types of summation methods can be selected:
    - Linear, the simplest method but generally the least accurate.
    - Quadratic, which combines the velocity components using the quadratic sum $\sqrt{x^2 + y^2}$.
    - Weighted, where at each point the velocity components are weighted based on the ratio between the local wind speed and the average wind speed. This method is preferrable when many wakes interact with each other, because of its good accuracy as it conserves momentum.
- Blockage effect model, whose structure is very similar to that of the previously described wake models, accounts for the loss of momentum—and therefore wind speed—caused by the turbine acting as a physical obstacle to the wind. The choice of this model becomes important when the flow around individual turbines is analysed in detail, but it does not significantly affect the results when considering large-scale wake effects.
- Deflection model, which calculates the deflection of the wake when the turbine is misaligned with the wind direction. Under nominal conditions, this model is not strictly necessary; however, if the analysis specifically focuses on the effects of misalignment and aims to optimize energy production through yaw control, then wake deflection becomes important.
- Rotor-average model: since calculating the velocity deficit at the rotor center does not yield accurate results, this model involves selecting specific points or zones within the swept area of the turbine where the deficit calculations are performed. Among the most common models:
    - AreaOverlapAvgModel, which considers the rotor section impacted by the wake of an upstream turbine. This is valid only for wake models of the top-hat type.

- GaussianOverlapAvgModel, which calculates the integral over the rotor area of the Gaussian wake of an upstream turbine. Valid only for wake models with a Gaussian profile.
- CGIRotorAvg, which, unlike the previous models, does not select areas but rather individual points defined by polar coordinates.
- GridRotorAvg, which builds a grid of points defined in Cartesian coordinates.

Once the most suitable model for our needs has been identified, to complete the setup it is necessary to define the geographic site and the specific turbine installed within the program. Defining the site involves specifying the wind speeds, directions, turbulence intensities, and the probabilities that different "triplets" occur. For each considered direction, the probability of a certain wind speed occurring can be represented using a Weibull distribution:

$$f(v;k;\lambda) = \left(\frac{k}{\lambda}\right)\left(\frac{v}{\lambda}\right)^{k-1}\exp\left(-\left(\frac{v}{\lambda}\right)^{k}\right)$$

where v is the wind speed, k is the shape factor, and λ is the scale factor. For the wind speed distribution, k is always bigger than 1, while λ equals to the mean wind speed. This distribution thus encompasses all possible scenarios within the given time period and is therefore used to define the site model, which can be selected from three options:

- UniformWeibullSite, which can be used when the wind follows a uniform Weibull distribution, a scenario that occurs in reality only over flat terrain without obstacles, resulting in a constant average wind speed at every point. This model is therefore used for offshore wind farms, as the sea typically exhibits these characteristics.
- WaspGridSite, which is used when wind speed distributions are not homogeneous, i.e., over non-flat terrain. To obtain this distribution, data must be derived using the WAsP software af3ter defining the terrain configuration where the wind farm is located.
- XRSite, the most flexible model, which can take as input a precompiled dataset to continuously define varying Weibull distributions. It is the most complex and is used for highly specific analyses.

To complete the model, it is eventually necessary to specify the characteristics of the turbine. These can be implemented using models available in the PyWake library, or a model can be built from scratch by defining the power curve and thrust

coefficient for each wind speed, then specifying the rotor height and diameter. This information is required to proceed with the calculation of the AEP of the entire wind farm.

2.3. FLORIS

FLORIS [10] (FLOw Redirection and Induction in Steady State) is a tool developed by the National Renewable Energy Laboratory (NREL) with the primary goal of optimizing wind farms and implementing various control strategies, taking into account the negative effects of turbulence and wake generated within a wind farm. Also written in Python, it consists of a package called *floris.core*, which contains the calculation algorithms, and the main package *floris*, which serves as an interface to visualize results and the control process, if applicable. The construction of the wind farm is carried out directly in the Python script, making it easier to modify the layout during development.

2.3.1. Wind Farm Models

Just like in PyWake, all calculations in FLORIS are based on a model that must be defined at the beginning of the script. The default model used is *FlorisModel*, but other subclasses of models are available, each differing slightly from the main one:

- *ParFlorisModel*: produces the same results but runs the code using parallelized calculation.
- *UncertainFlorisModel*: adds uncertainty in the definition of wind directions among the inputs, thus providing different results compared to the previous two models.
- *ApproxFlorisModel:* is also used to simplify data processing by setting a resolution, making the process much faster when using large datasets with minor variations.

Once the model is selected, the FLORIS interface allows users to change variables within the model using the *fmodel.set()* command, from the layout to wind characteristics, and including the various types of operation model for the turbines. The function *operation_model* indicates models that define how each turbine is operating. FLORIS offers several operation models:

- "*simple*": considers the power curve and thrust coefficient as the only variables for calculating energy production. It is the standard model used for baseline assessment.

- "*cosine-loss*": unlike the previous model, it includes losses due to turbine misalignment relative to wind direction.
- "*simple-derating*": allows for applying power setpoints to avoid overloading the turbine and prevent degradation.
- "*mixed*": combines features from the previous two models.
- "*awc*": a model that controls turbine yaw angles to minimize speed reductions caused by wakes (Active Wake Control).
- "*peak-shaving*": reduces peak loads acting on the blades.

2.3.2. Wake Deficit Models

As for the wake model, FLORIS allows it to be defined from its internal library and easily called during initialization. FLORIS offers fewer options compared to PyWake in this regard, as it supports only the Jensen model (top-hat) and a few Gaussian-shaped models: Cumulative Curl, Empirical Gaussian, and GCH. However, FLORIS places particular emphasis on wake deflection: in fact, each wake model includes a built-in deflection model, unlike PyWake, which allows the user to independently define the deflection model between top-hat and gaussian approaches. Therefore, although FLORIS provides fewer general options than PyWake, calling a model from the FLORIS library enables complete wake modelling, including deflection behaviour.

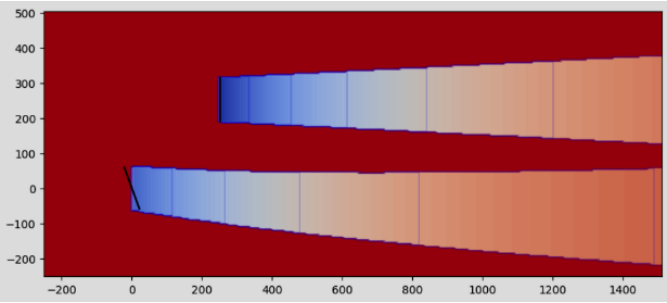

Figure 5: Wake modelling using Jensen model (FLORIS)

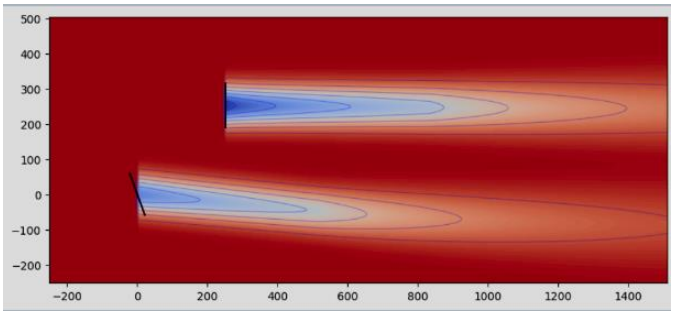

Figure 6: Wake modelling using GCH model

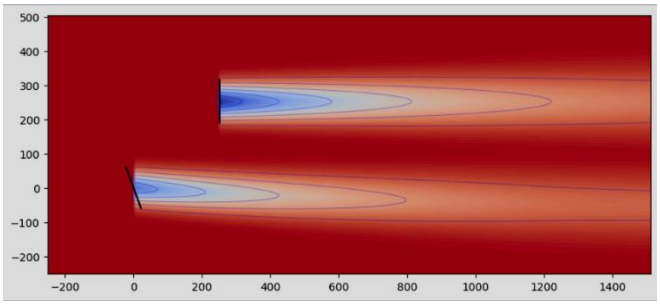

Figure 7: Wake modelling using the Empirical Gaussian model

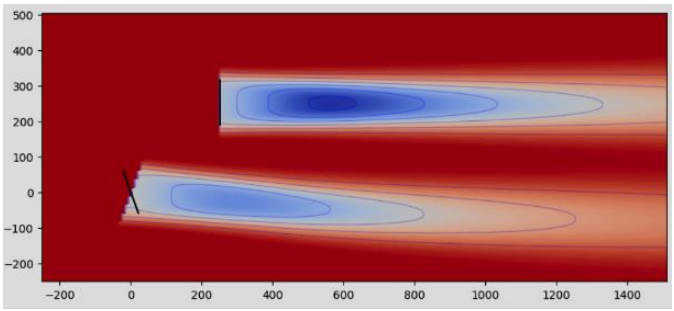

Figure 8: Wake modelling using Cumulative Curl model

Regarding site wind information, FLORIS essentially allows integration through two objects:

- WindTIRose: represents wind rose data, plus turbulence intensities as a separate string. The occurrences therefore have three dimensions, representing the probability of each "triplet" occurring.
- WindRoseWRG: allows extraction of wind rose data from a Wind Resource Grid (.WRG) file, which can be generated by software such as WAsP. This solution is not only very fast but also highly accurate.

Finally, for turbine setup, the FLORIS *turbine_library* module is used, which contains default turbine models for performing analyses. FLORIS includes useful objects such as *TurbineInterface*, which allows graphical visualization of the

characteristics of the selected turbine, such as power curves or thrust coefficients, depending on where the turbine is placed, and *TurbineLibrary*, useful for loading multiple turbines simultaneously and comparing different configurations on the same graph.

2.3.3. Control Strategies

Once the model is set up with all its specifications, FLORIS, beyond calculating Annual Energy Production (AEP) and visualizing wake propagation through space, is particularly effective for implementing control strategies, which are essentially the main reasons this software is widely used:

- **Yaw Optimization**: optimizing a wind farm by modifying the yaw angles of the turbines is the main purpose for which FLORIS is used. The *YawOptimizationSR* function calculates the optimal yaw for each turbine using the so-called Serial-Refine method: starting from the most upstream turbine to the most downstream, the algorithm adjusts one turbine at a time to find the angle that maximizes energy production (Serial Pass), comparing 0° with a set of discrete yaw angles (e.g., -20°, -10°, 0°, +10°, +20°). Once this process is completed for all turbines, the algorithm restarts from the first turbine (Refine Pass) and fine-tunes the result by testing yaw angles closer to the one previously selected in the Serial Pass (e.g., if +10° was found optimal, the Refine Pass tests +5°, +7.5°, +10°, +12.5°, +15°). This method is very fast because it limits the number of iterations, yet it yields excellent results even when compared to more computationally expensive approaches. Yaw optimization is useful especially in wind farms where turbines are not ideally arranged (e.g., too close or aligned in the wind direction), as deflecting the wake can allow downwind turbines to operate in less reduced wind conditions. FLORIS also supports two additional yaw optimization functions, *YawOptimizationScipy*, which uses SciPy[21]'s optimize function, and *YawOptimizationGeometric*, that computes optimal yaw based on rotor geometry. These methods are respectively more and less computationally expensive than *YawOptimizationSR*.

- **Turbines Disabling**: During model setup, FLORIS allows defining turbine disabling combinations to evaluate wake behaviour and overall farm productivity in cases where one or more turbines are shut down.

- **Pitch Control**: Like yaw, pitch also plays a fundamental role in wake propagation. In Active Wake Control (AWC) strategies, pitch is adjusted to enhance wake mixing downstream of the turbines, thereby reducing wind speed deficits. Naturally, adjusting the pitch angle results in a power reduction for the turbine, which is no longer oriented for optimal wind capture. In the existing wake models within FLORIS, there are *helix** coefficients *(a, b,* and *c)* that describe the turbine's power output under AWC as a function of its baseline power:

$$P_{\mathrm{AWC}} = P_{\mathrm{baseline}} \cdot (1 - (b + c \cdot P_{\mathrm{baseline}}) \cdot A_{\mathrm{AWC}}^{a})$$

  with A_{AWC} indicating the maximum amplitude of the pitch angle, which can be set during the model configuration. AWC in FLORIS can be simulated using the "*awc*" operation model.

- **Productivity assessment with uncertain wind conditions**: by specifying the standard deviation of the wind direction in the setup of the *UncertainFlorisModel*, more realistic analyses can be performed. For example, this allows the evaluation of AEP variability under maximum or minimum wind speed conditions.

- **Derating turbines**: derating strategies (setting power setpoints that define a new nominal power output for the turbine) are commonly used. Derating is beneficial for several reasons, such as reducing aerodynamic loads on the blades during high wind speeds or turbulence, which could cause long-term damage, or reducing noise emissions, especially important in areas requiring acoustic control. Setpoints are selected directly within the *fmodel.set()* function and can be applied to all or only some turbines. Derating control in FLORIS is simulated using the "*simple-derating*" operation model.

- **Peak Shaving**: This is a common control strategy used to reduce structural loads caused by high thrust forces on the blades. The strategy involves lowering the thrust coefficient at wind speeds near the peak of the thrust curve (usually corresponding to the lower end of the rated power zone). In this region of the curve, the turbine power is calculated using a specific equation based on nominal values of P' (modified power), C_T' (modified

thrust coefficient), and a' (axial induction factor). New values of a and C_T are then derived using the standard actuator disk theory relationships:

$$P = \frac{C_T(1-a)}{C_T'(1-a')}P'$$

To implement peak shaving, the use of the "*peak-shaving*" operation model is required.

- **Layout Optimization**: Using the *LayoutOptimizationScipy* function, FLORIS can determine the optimal layout of wind farm turbines in terms of AEP, restricting the search for ideal positions within predefined boundaries. Turbines are generally placed equidistant from each other and near the edges of the area defined by the boundaries, with some spatial adjustments based on the wind rose occurrence patterns.

- **Load Optimization**: The load on each turbine due to turbulence must also be evaluated economically. The Variable Operational Cost (VOC) represents the annual cost of maintaining a turbine affected by Load Turbulence Intensity (LTI). Both parameters can be assessed in FLORIS using *compute_lti()* for calculating Load Turbulence Intensity, and *compute_turbine_voc()* for estimating the turbine's operational cost. From this perspective, operating turbines at reduced rated power using the "*simple-derating*" operation model allows users to compare maintenance costs when operating at full power versus reduced power.

3. Implementation of models

Understanding the structure of a software tool like PyWake can be very useful when aiming to find the optimal setup for accurate analysis. Therefore, in the following sections, some of the various mentioned models are compared using a basic case study: a fictitious wind farm with 16 turbines arranged in staggered columns. The four rows of turbines, each with a 250-meter rotor diameter, are spaced equidistantly, with a minimum distance between rows set to allow wind speed recovery—approximately eight rotor diameters. The turbines within each row are also evenly spaced. After importing the wind conditions and turbine specifications, the analysis was carried out by changing the input conditions for each scenario.

3.1. Distances

The layout of a turbine can significantly affect the turbulence caused by wakes. A very dense layout will prevent the wind from recovering its speed between turbines, potentially leading to significant velocity losses. Conversely, having more space between turbines helps to limit turbulence to a smaller area around each turbine. In the following scenarios, the four rows of turbines were spaced at d= 500 m, 1000 m, and 2000 m from one another, with an initial wind speed of 15 m/s coming from West.

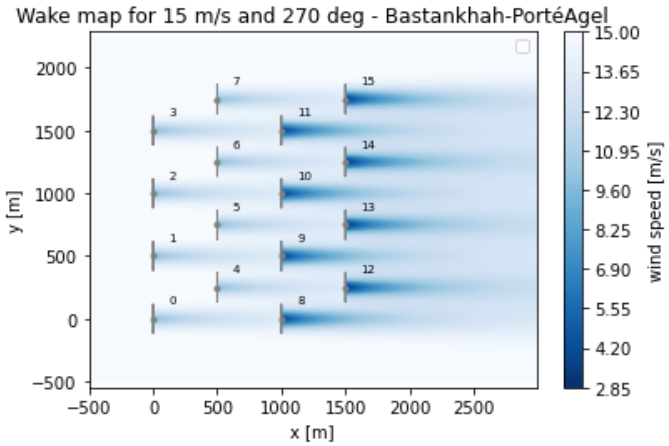

Figure 9: Wake map for d = 500m (PyWake)

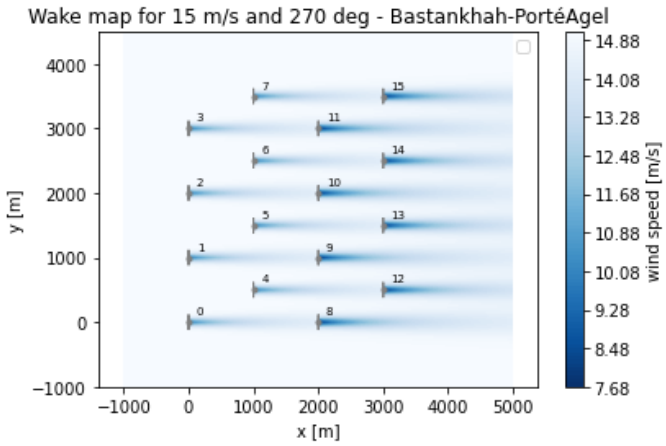

Figure 10: Wake map for d = 1000m (PyWake)

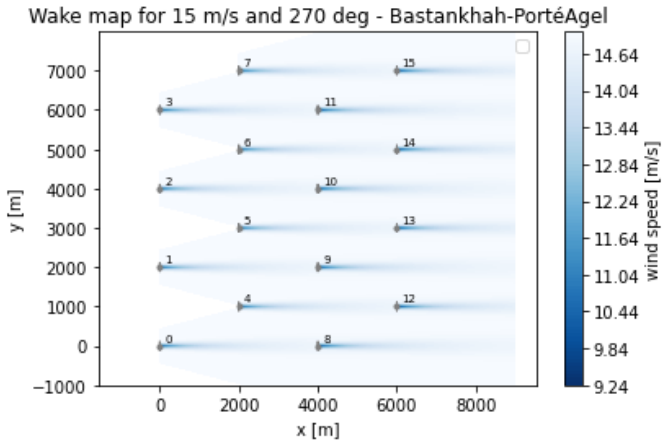

Figure 11: Wake map for d = 2000m (PyWake)

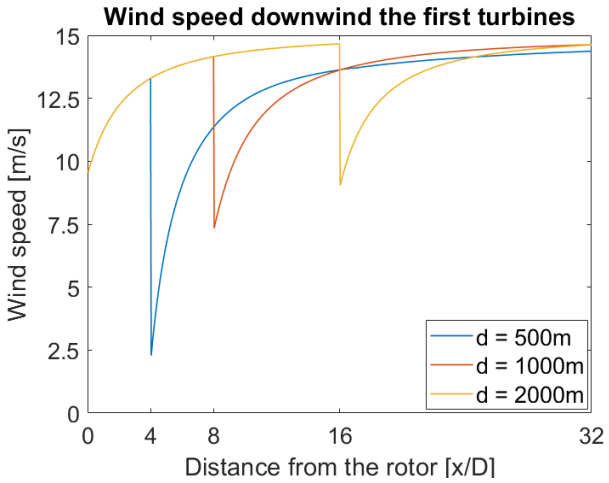

Figure 12: Comparison among wind profiles

In the first case, wind speed is reduced by one-fifth after the first turbines and by up to 90% after the last ones. In the second case, the wake results in a wind speed that is half of the original. Finally, in the third case, which will be considered the standard case in the following sections, the turbines are spaced far enough apart to allow the wind speed to recover after the first two rows, resulting in uniform wakes throughout the wind farm. It becomes clear that spacing turbines sufficiently provides a significant advantage in terms of turbulence mitigation. On the other hand, using too much space is not always feasible in real-world scenarios; therefore, wake analysis is valuable for optimizing turbine placement efficiently within limited space. The same three layouts were also implemented in FLORIS:

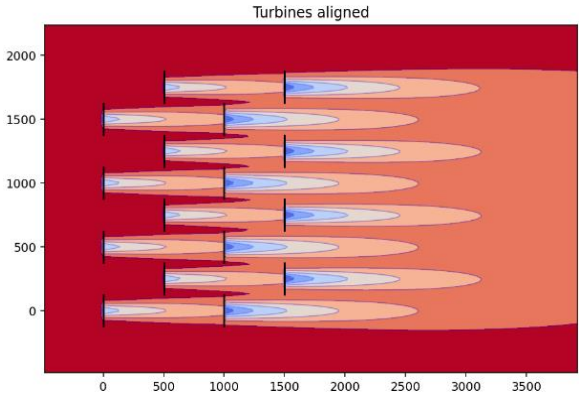

Figure 13: Wake map for d = 500m (FLORIS)

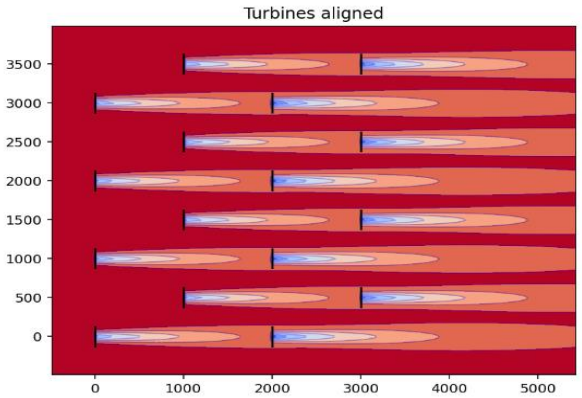

Figure 14: Wake map for d = 1000m (FLORIS)

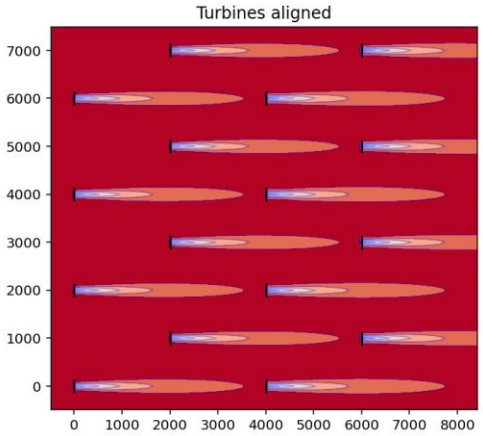

Figure 15: Wake map for d = 2000m (FLORIS)

As can be observed, FLORIS provides a much more simplified default visualization, but it is sufficient to outline the wake behaviour in this basic case: as the distance between rows increases, the wind is able to recover more easily, thereby reducing downstream turbulence.

3.2. Wake Models

In recent years, an increasing number of Gaussian-shaped wake models have been developed, with slight differences between them. Here, two of them are presented: the Bastankhah model and the Zong model, along with the top-hat model by Jensen:

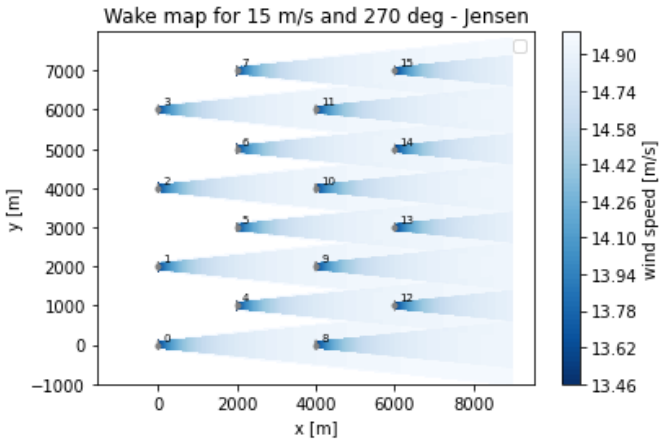

Figure 16: Wake map for Jensen model

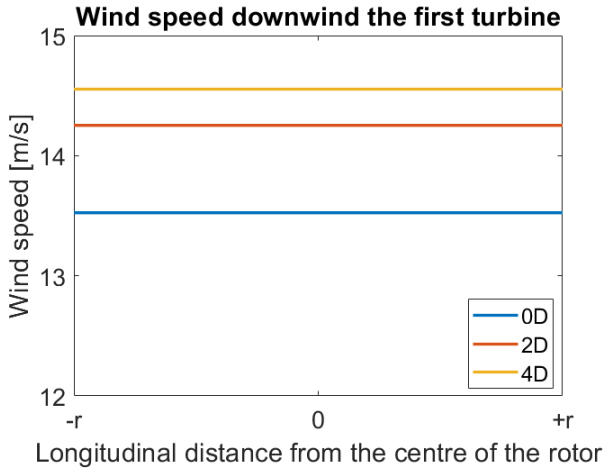

Figure 17: Comparison of wind profiles behind the rotor for Jensen model

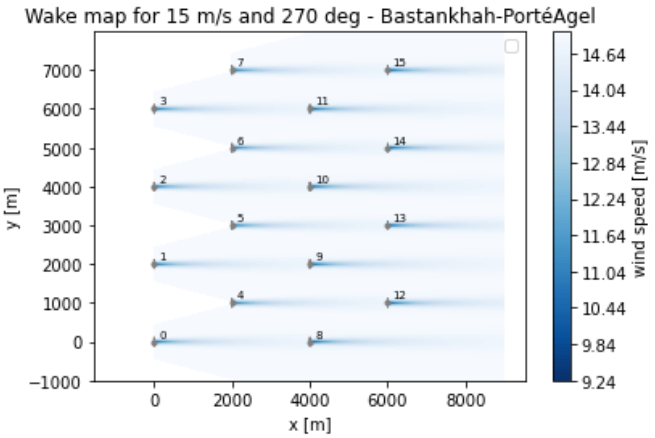

Figure 18: Wake map for Bastankhah model

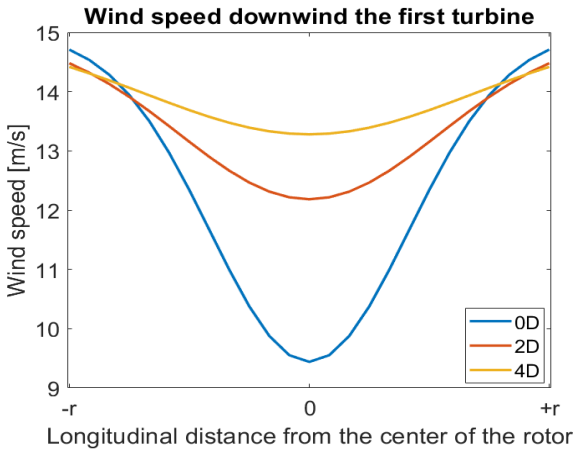

Figure 19: Comparison of wind profiles behind the rotor for Bastankhah model

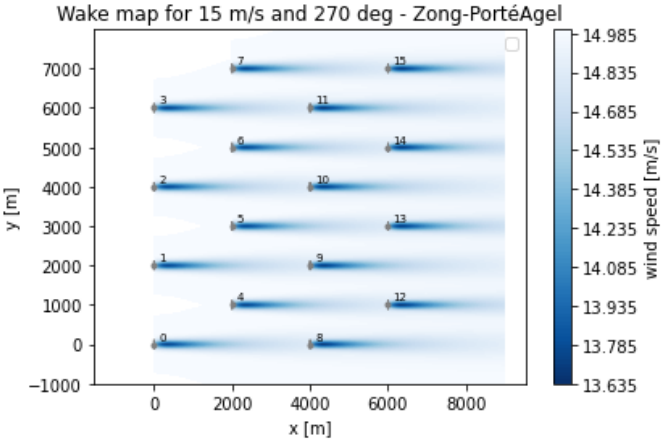

Figure 20: Wake map for Zong model

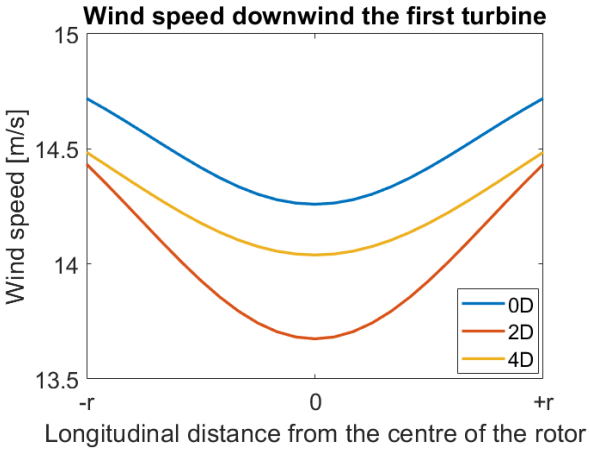

Figure 21: Comparison of wind profiles behind the rotor for Zong model

The Jensen model models the far wake more accurately. In fact, as seen in the figure, the effects of the initial wakes are still visible even after the last downwind turbines. However, when it comes to the near wake, Jensen is less accurate, detecting only a limited velocity drop, and only very close to the turbine (see previously included graphs). The near wake is better captured by Gaussian models like Bastankhah, which show a much greater velocity deficit near the turbine, although it recovers quickly after just a few rotor diameters (D), returning to the original values and effectively eliminating far wake effects.

Lastly, the Zong model, introduced in 2020, appears to be a middle ground: while the minimum wind speeds in the near wake are close to the original, it affects a much larger area, thereby extending the wake more significantly than the Bastankhah model.

It becomes clear that the choice of model depends on the specific phenomenon one intends to analyze: although Gaussian models are generally preferred over Jensen for their higher accuracy, differences exist among the Gaussian models themselves. Some are better suited for analyzing wake effects on the turbines themselves (near wake and fatigue), while others yield more relevant results for evaluating overall turbulence propagation across a wind farm (i.e., the transition zone between near and far wake).

In FLORIS, where the available wake models are more limited, the downwind behaviour of the top-hat model and the Empirical Gaussian model is visualized:

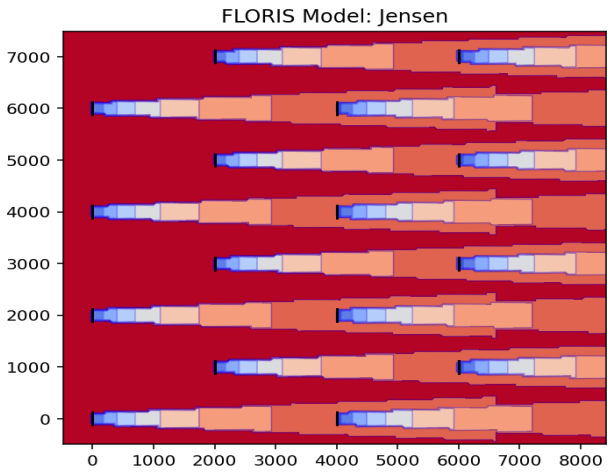

Figure 22: Wake map for Jensen model (FLORIS)

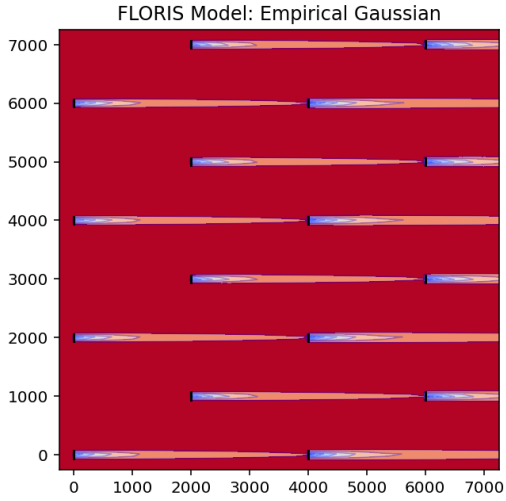

Figure 23: Wake map for Empirical Gaussian model

3.3. Velocity

3.3.1. Bastankhah Gaussian Wake model

Each wake model also responds differently to changes in wind speed during simulations. Simulations were carried out using the Bastankhah model with wind speeds of 12, 13, and 14 m/s:

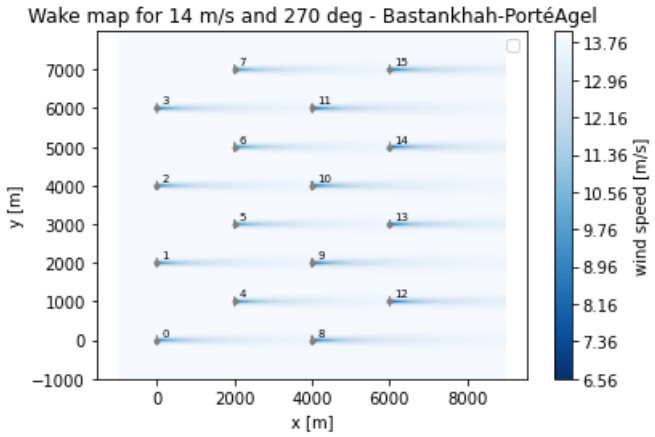

Figure 24: Wake map for 14 m/s wind speed for Bastankhah model

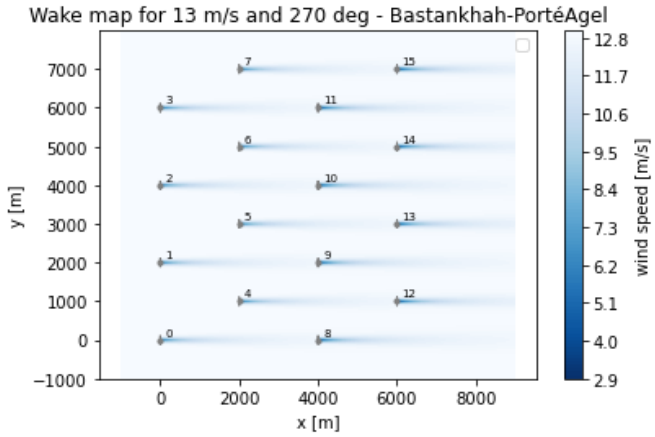

Figure 25: Wake map for 13 m/s wind speed for Bastankhah model

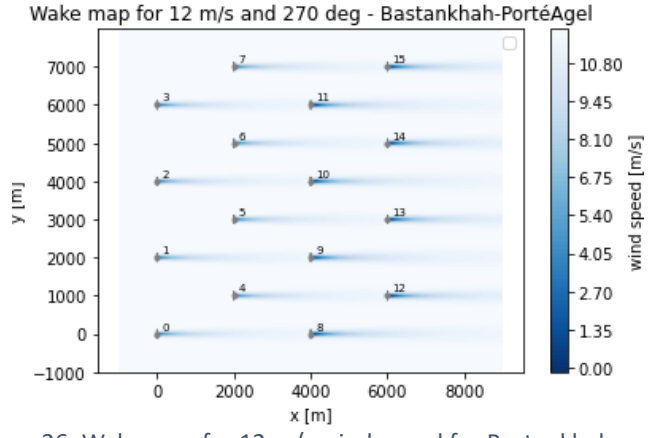

Figure 26: Wake map for 12 m/s wind speed for Bastankhah model

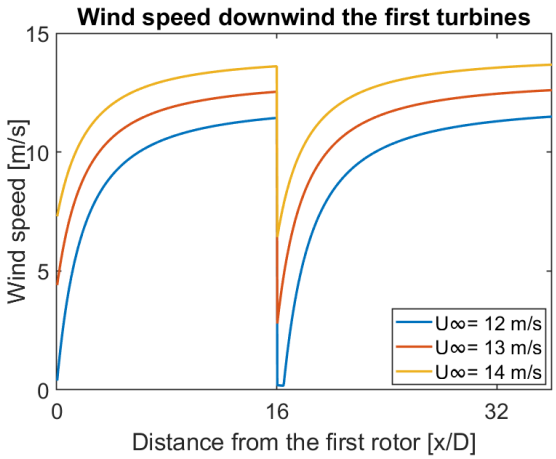

Figure 27: Comparison among wind profiles

In the base case at 15 m/s, the minimum wind speed in the near wake stabilized at 9.24 m/s. By reducing the wind speed by 1 m/s at a time, the maximum velocity deficit became increasingly significant, eventually reaching stall conditions, with 0 m/s in the near wake at a freestream wind speed of 12 m/s. It is clear that the assumed layout in this case prevents wind speed recovery upstream of the last turbines, which is why using this wake model led to very different results for small changes in wind speed.

3.3.2. Zong Gaussian Wake Model

The Zong model, on the other hand, limits the velocity drops observed in the Bastankhah model, reaching a minimum wind speed of 5.25 m/s with a freestream wind speed of 10 m/s, and thus proves to be less sensitive to variations in wind speed:

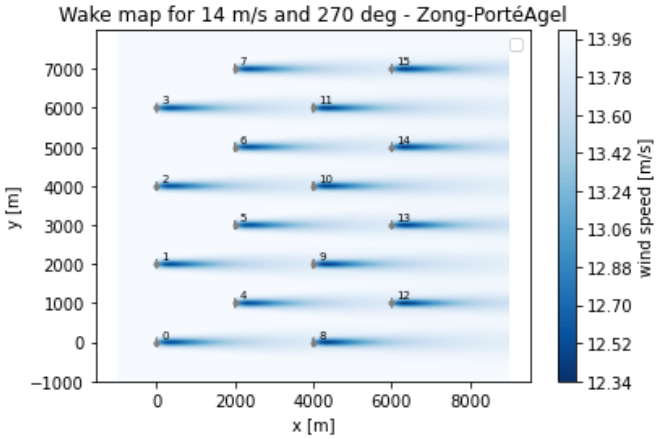

Figure 28: Wake map for 14 m/s wind speed for Zong model

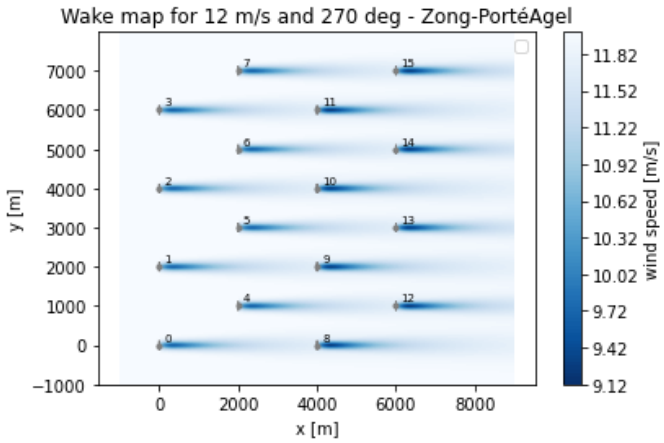

Figure 29: Wake map for 12 m/s wind speed for Zong model

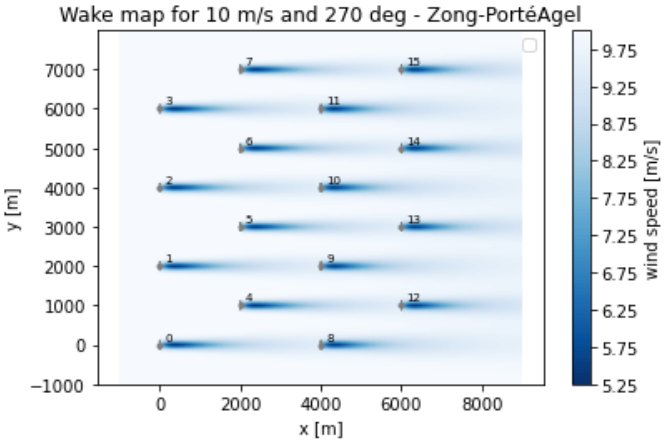

Figure 30: Wake map for 10 m/s wind speed for Zong model

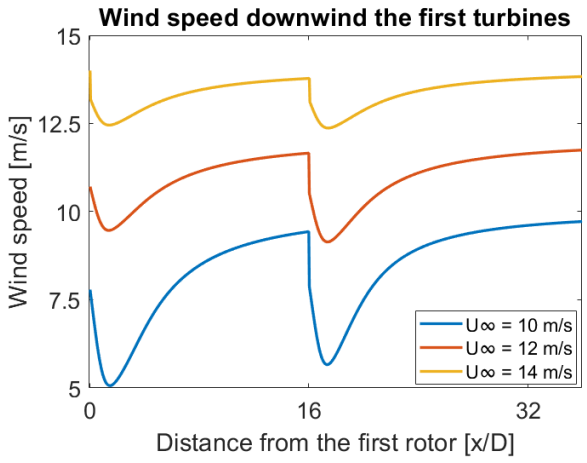

Figure 31: Comparison among wind profiles

3.4. Superposition Models

The three previously mentioned superposition models (LinearSum, WeightedSum, and SquaredSum) were applied, using a wind speed of 15 m/s and the Zong wake model.

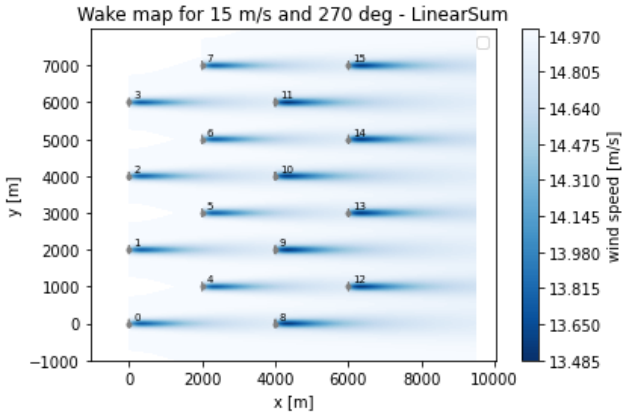

Figure 32: Wake map using LinearSum model (Zong)

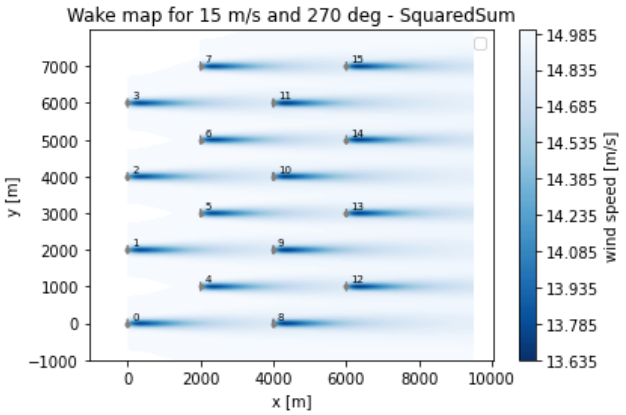

Figure 33: Wake map using SquaredSum model (Zong)

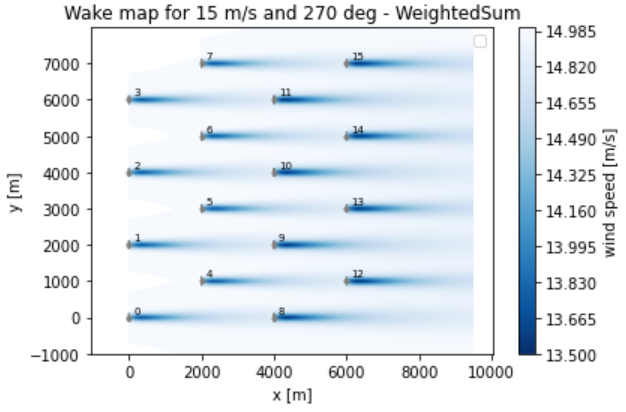

Figure 34: Wake map using WeightedSum model (Zong)

With these inputs, the differences are essentially negligible; however, it can be observed that the models produce more varied results when the turbine layout is made denser and the wind speed is reduced to 12 m/s.

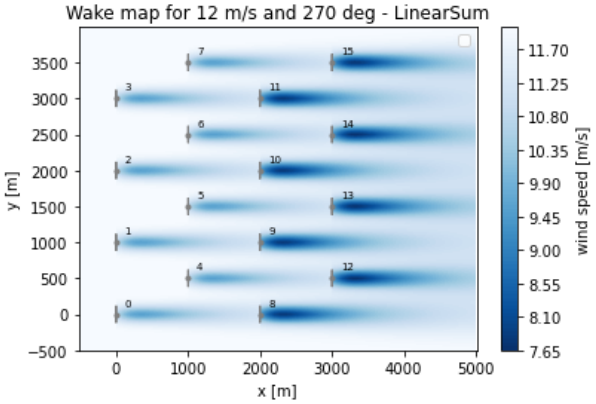

Figure 35: Wake map using LinearSum model with new layout (Zong)

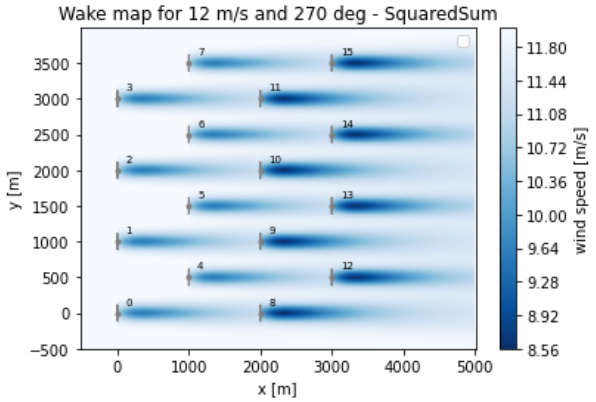

Figure 36: Wake map using SquaredSum model with new layout (Zong)

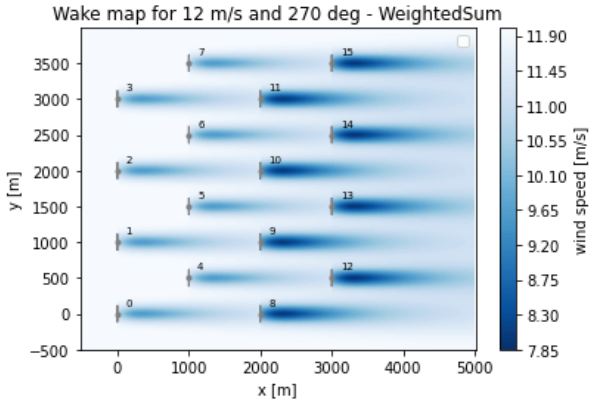

Figure 37: Wake map using WeightedSum model with new layout (Zong)

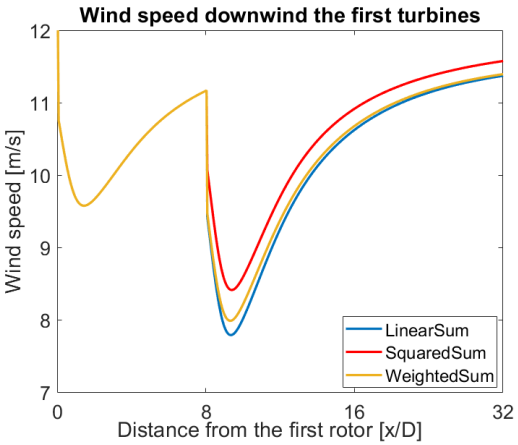

Figure 38: Comparison among wind profiles

The WeightedSum differs from SquaredSum in terms of velocity deficit, but more importantly, it is more accurate in assessing the greater wake intensity in the last two rows of turbines. In fact, SquaredSum, designed primarily to eliminate the possibility of negative wind speeds, often proves to be inconsistent for accurate wake simulation [22]. LinearSum, on the other hand, aligns more closely with WeightedSum in this regard. Although this model does not conserve momentum along the wake as accurately, with the Zong model, the two superposition methods produce comparable results.

That said, the difference in how the wake develops spatially becomes more apparent in the following simulations, carried out using the Bastankhah wake model with a wind speed of 10 m/s:

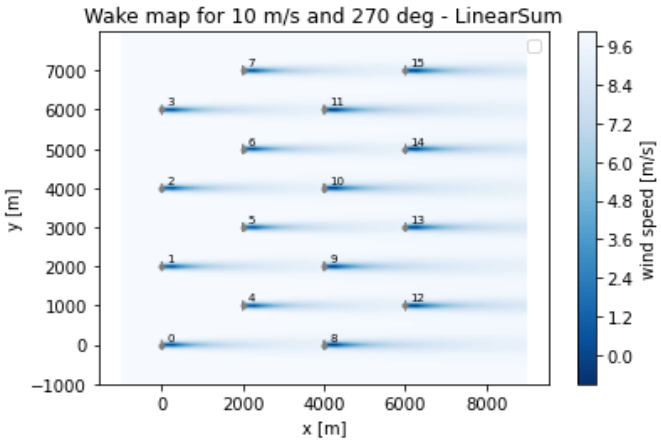

Figure 39: Wake map using LinearSum (Bastankhah)

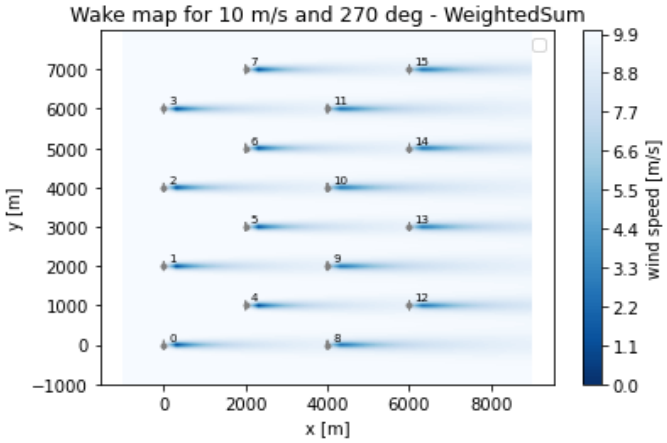

Figure 40: Wake map using WeightedSum (Bastankhah)

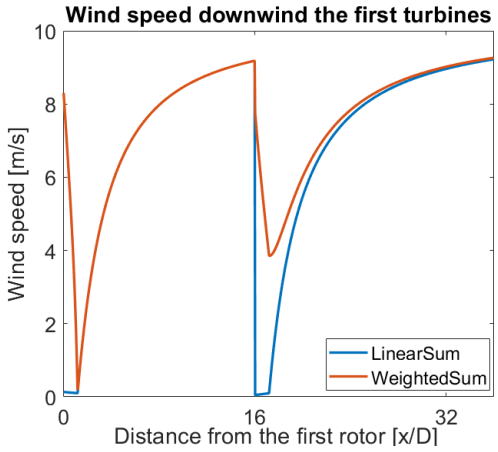

Figure 41: Comparison between wind profiles

It is therefore clear that, unlike the Zong model, for the Bastankhah model it is preferable to use WeightedSum, even though it is more computationally expensive. It should also be noted that these two superposition models, unlike SquaredSum, can produce negative wind speeds. The use of the "use_effective_ws=True" option when defining the model allows this issue to be overcome by considering, point by point, the effective wind speed, taking into account the influence of upstream turbines.

Table 1: Summary of models analyzed

Model	Year	Most precise wake zone	Computational time (in this case)	Preferrable superposition model
Jensen	1983	far	~ 0.90 s	SquaredSum
Bastankhah	2014	near	~ 1.30 s	WeightedSum
Zong	2020	mid	~ 1.60 s	LinearSum

3.5. Rotor-Average Models

The default wind direction considered so far does not allow differences between the various models to be observed, since each turbine is hit by the wake of the upstream turbine in a perfectly centered manner. By considering a different direction (in this case, 300 degrees), turbines can be grazed by a wake that is asymmetric relative to the rotor, thus causing differences between GridRotorAverage and CGIRotorAverage. For simple cases like this, the GaussianOverlap model can be replaced without significant changes by the CGI model, which uses reference points arranged in a polar manner, all equidistant from the center.

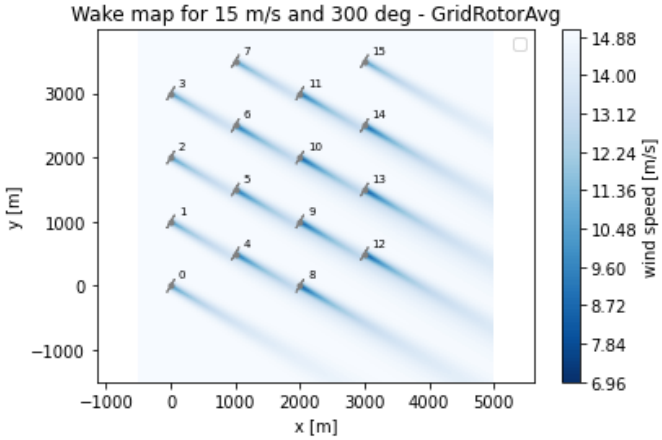

Figure 42: Wake map using GridRotorAvg model

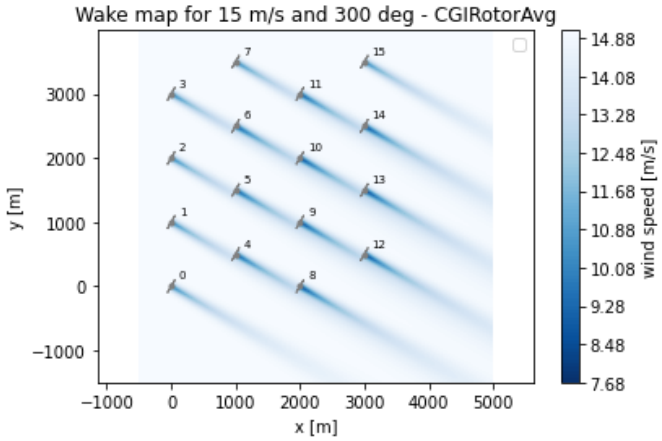

Figure 43: Wake map using CGIRotorAvg model

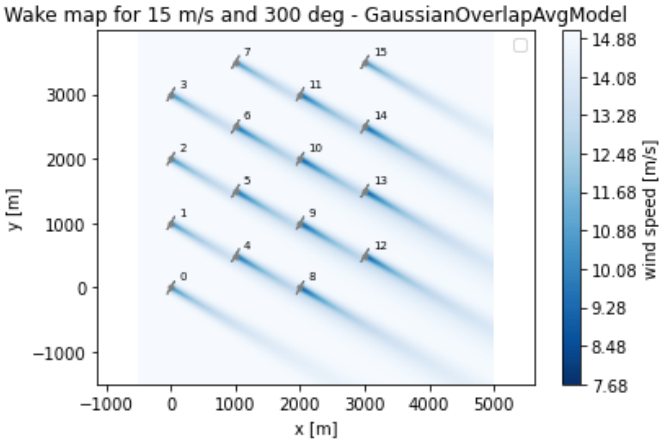

Figure 44: Wake map using GaussianOverlapAvg model

For Gaussian-section wake models, the preferred choice is GaussianOverlap, since it encloses the exact area where the wake impacts the rotor. As shown in the plots, an interesting alternative, less demanding in terms of computational resources, is to use symmetrically placed reference points (CGI).

3.6. Deflection Models

When it comes to deflection models, FLORIS is more compelling, as it implements them with particular care in order to optimize the AEP. This goal is achieved by finding the optimal yaw angle for each turbine in the wind farm, pairing each wake deficit model with a corresponding deflection model. The wake is therefore intentionally deflected to avoid directly impacting certain downstream turbines, allowing for wake recovery and improving long-term energy production.

The layout considered in the previous cases is now implemented in FLORIS with three wake deficit/deflection models, using a yaw angle of +20° for the second row of turbines and of -20° for the fourth row:

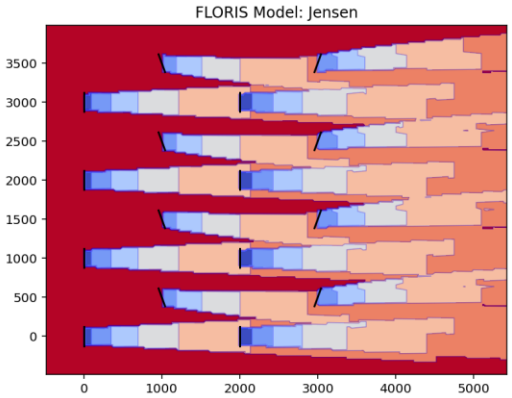

Figure 45: Wake map with Jensen deflection model effects

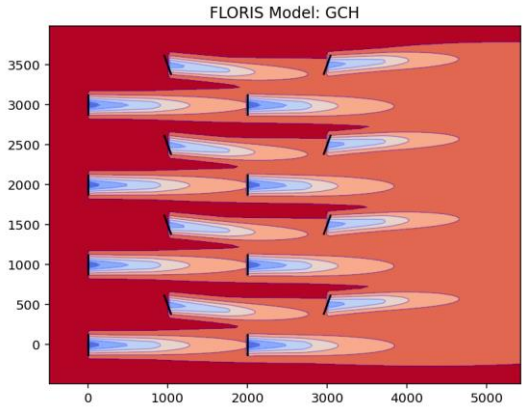

Figure 46: Wake map with GCH deflection model effects

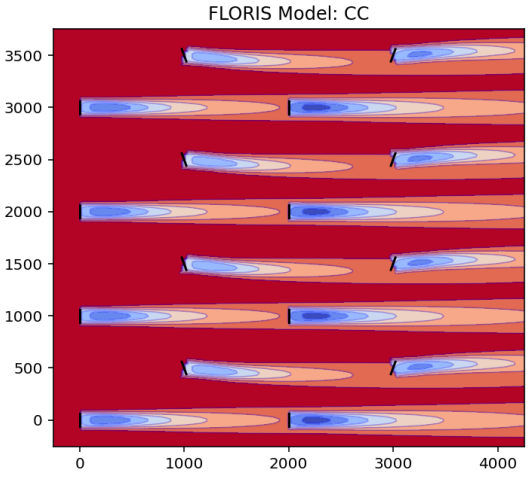

Figure 47: Wake map with Cumulative Curl deflection model effects

The Jimenez model, when paired with the Jensen wake model, naturally produces a deflection that preserves the top-hat profile. The other two models, however, maintain a Gaussian shape: the GCH model closely resembles the classical Bastankhah model (with a significant deficit near the turbine), while the CumulativeCurl model is more similar to Zong's model (with a more pronounced deficit occurring at a distance of 1D–2D downstream from the rotor).

PyWake includes only the Jimenez deflection model and the GCLHill model, which is essentially equivalent to the GCH model implemented in FLORIS. Since these two models can be respectively associated with the Jensen model and with all Gaussian-profile wake models in PyWake, the aim is now to describe an algorithm that enables AEP optimization in PyWake, while making it adaptable to wake models that are not available in FLORIS.

4. Integration PyWake-FLORIS

4.1. Algorithm design

The algorithm was structured starting from the definition of the model, so the site and its wind rose, the turbine (in this case, an IEA 15 MW turbine [23]), the wake model, and the corresponding deflection model. When a deflection model is implemented, the wind farm simulation command requires the yaw angles of each turbine as input. To simulate the baseline case, an initial yaw angle of 0° was set for each turbine, thus obtaining the AEP value of the wind farm without yaw control as output. Subsequently, an iterative loop was built with the goal of finding the optimal yaw orientation for each turbine (within the limits of -20° to +20°) for every considered wind direction (from 0° to 330°, in 30° increments), with the goal of maximizing the power extracted from each turbine, and therefore the overall AEP.

This was made possible by using the `minimize` function from SciPy: first, an objective function, which returns the negative of the AEP, was created; then, the `minimize` function was used to find the minimum of the negative AEP (which corresponds to the maximum absolute value of the AEP), by simulating the model and iterating, for each direction, through all possible yaw combinations within the predefined limits. Therefore, from the process just described, 12 combinations of 16 yaw angles are obtained in this case (12 wind directions x 16 turbines).

Below there is an example of how the wind farm under consideration appears on PyWake before and after applying yaw control for wind with 10 m/s speed coming from the North:

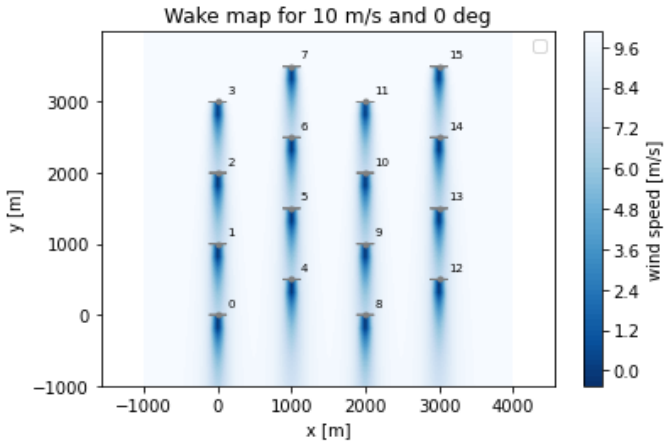

Figure 48: Wake map without deflection angles for any turbine

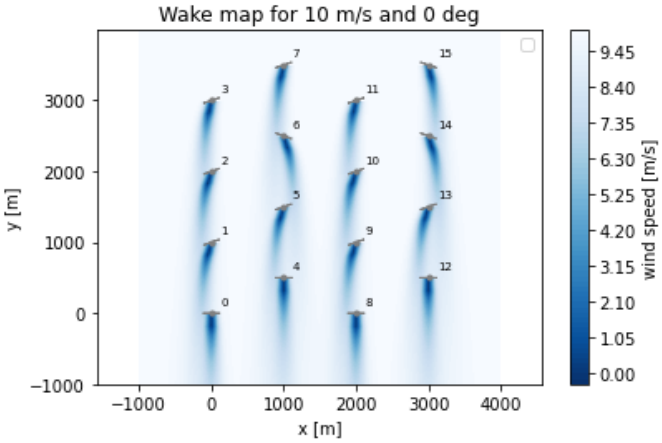

Figure 49: Wake map with deflection angles for some turbines

In the example provided, the same layout used in the previous chapter's example was maintained, along with the Bastankhah wake deficit model and the GCLHill deflection model, with the goal of finding the optimal yaw using the previously described method.

4.2. Base Case Results

The developed script provides, as a visual output, two maps that show for which wind directions and speeds the yaw control leads to an improvement in energy production, and for which it does not yield any benefits. Every rectangle in the map represents the difference between the sums of the powers of all turbines, after and before the yaw optimization, at a determined wind speed (x axis) and wind direction (y axis):

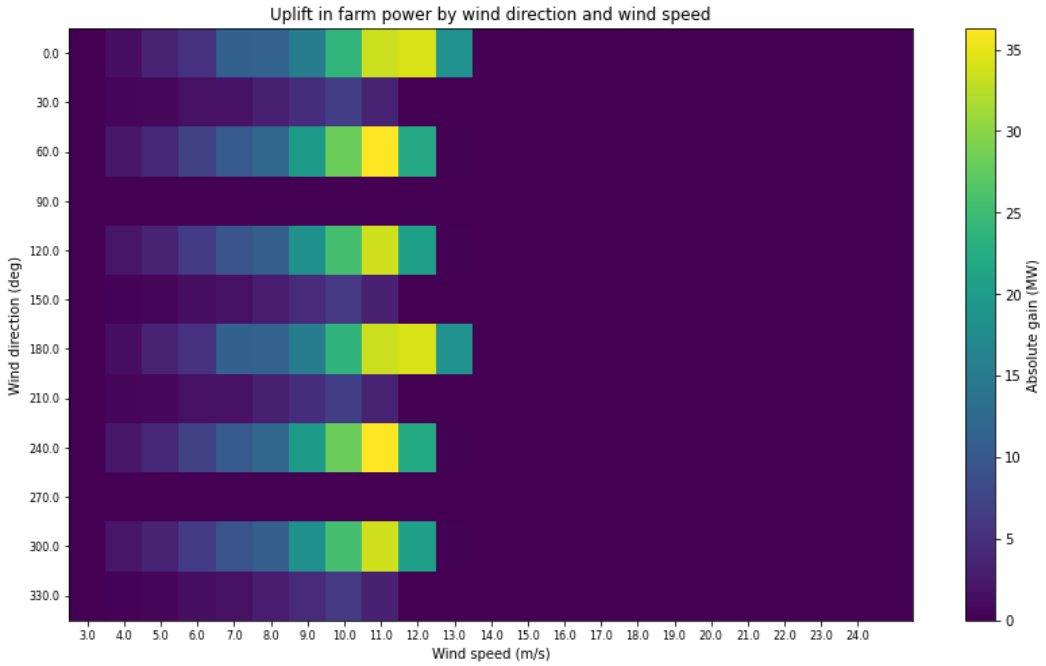

Figure 50: Absolute gain in AEP for each wind speed and direction

From the map, it is clear that yaw control yields excellent results for wind speeds around 11 m/s, with peaks in total power increase reaching up to 35 MW. This is noteworthy considering that the maximum rated power of the wind farm is 240 MW (15 MW × 16 turbines), which, according to the turbine's power curve, is achieved at wind speeds equal to or greater than 11 m/s.

The absolute gain naturally decreases as wind speed drops, since even under optimal conditions, the extractable power is lower due to the limits set by the power curve. But relative gain for this kind of speeds is higher, because even low absolute gains generate high percentage increases. Below are two examples illustrating the different wake behaviours—and thus the downwind wind speeds—for freestream wind speeds of 8 m/s and 20 m/s.

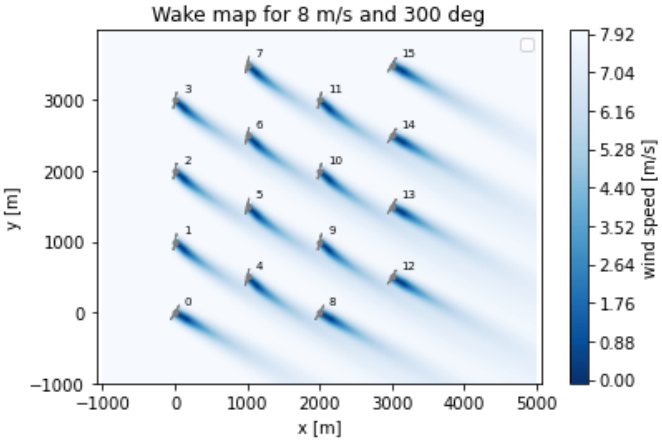

Figure 51: Deflection effects for low wind speeds

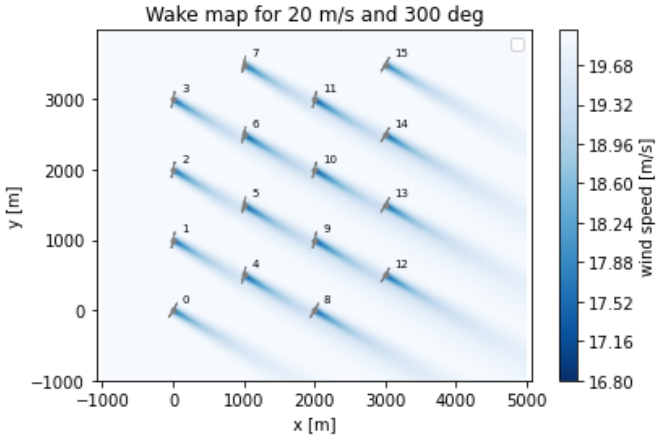

Figure 52: Deflection effects for high wind speeds

From these plots, it can be observed that the effect of yaw control is more noticeable in terms of wake deflection at lower wind speeds (the wake tends to "bend around" the downwind turbine), while it is almost imperceptible at higher speeds.

The consequences of this phenomenon are visible on the coloured map, where a sort of cut-off appears for wind speeds above approximately 13 m/s. This occurs because, as discussed in previous sections, higher wind speeds more easily allow the wake to recover downwind flow when Gaussian-shaped wake models are used.

Therefore, if the freestream wind speed is already high, all turbines are impacted by a sufficiently quick airflow to reach rated power even without the need for optimal yaw angles. For this reason, the map shows zero gain for all wind speeds above 13 m/s across all directions.

In fact, from a practical wind farm operation perspective, yaw control strategies are typically not implemented when wind speeds exceed 14 m/s (a common rule of thumb), as they offer no tangible benefit in those conditions.

It is also possible to observe how the relative gain (as a percentage of the baseline power) varies:

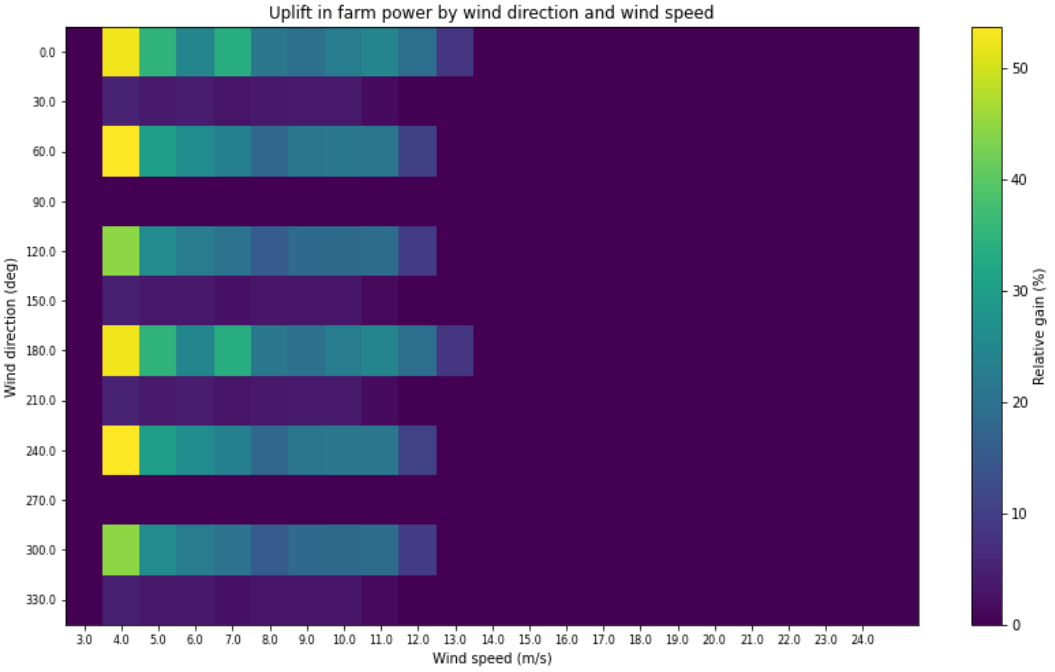

Figure 53: Relative gain in AEP for each wind speed and direction

Here, one can see that the percentage increase is actually more significant at lower wind speeds, reaching up to +50%. In contrast, the cases that showed the highest absolute gain translate to a +20% to +30% increase when viewed in relative terms. For higher wind speeds, the cut-off behavior is analogous to what was previously discussed.

Finally, the algorithm compares the initial AEP with the optimized AEP as the final result, highlighting the corresponding percentage increase. To perform this comparison accurately, it is of course necessary to import the wind data of the reference site, in order to realistically reproduce the full distribution of wind directions and speeds over a year. Importing data from a random sea site, this layout gave the following results:

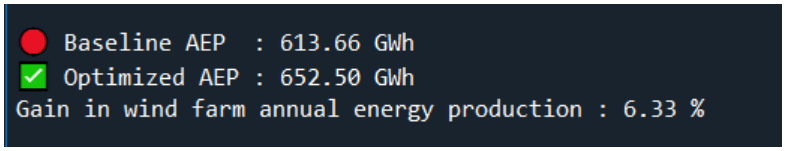

Figure 54: Results from the script

5. Case Study

5.1. Wind Resource Assessment

The previously described methodology is to be applied to a specific case study, in order to assess the potential post-construction wake effects. The case involves an offshore wind farm consisting of 32 wind turbines, for a total installed capacity of 480 MW. The selected turbine for each wind generator is the IEA 15MW, with a rotor diameter of 240 meters and a hub height of 150 meters. The power curve and thrust curve are shown below.

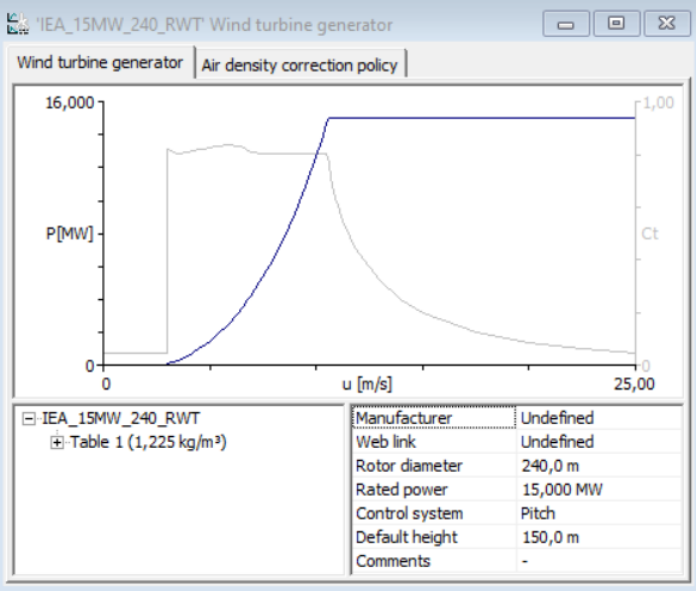

Figure 55: IEA 15 MW turbine specifics (from WAsP)

The selected site is located in the southern Adriatic Sea, off the coast of Barletta province. To assess the wind resource of the reference site, the WAsP software was used. Developed by DTU, WAsP is a framework that enables the modelling of the wind resource at a given site, allowing for the estimation of annual wind farm productivity.

Using the Global Wind Atlas [24], which contains ERA5 [25] datasets, the annual distribution of wind directions, intensities and their frequencies can be extracted

and represented as a wind rose. Once this wind rose is imported into WAsP, the software models the local wind climate at a resolution of 200 meters above sea level, across five different heights (10, 50, 100, 150, and 200 meters a.s.l.). Then, using WAsP Map Editor, the site can be characterized in terms of roughness and orography. However, since the wind farm is offshore, these two factors are not taken into consideration.

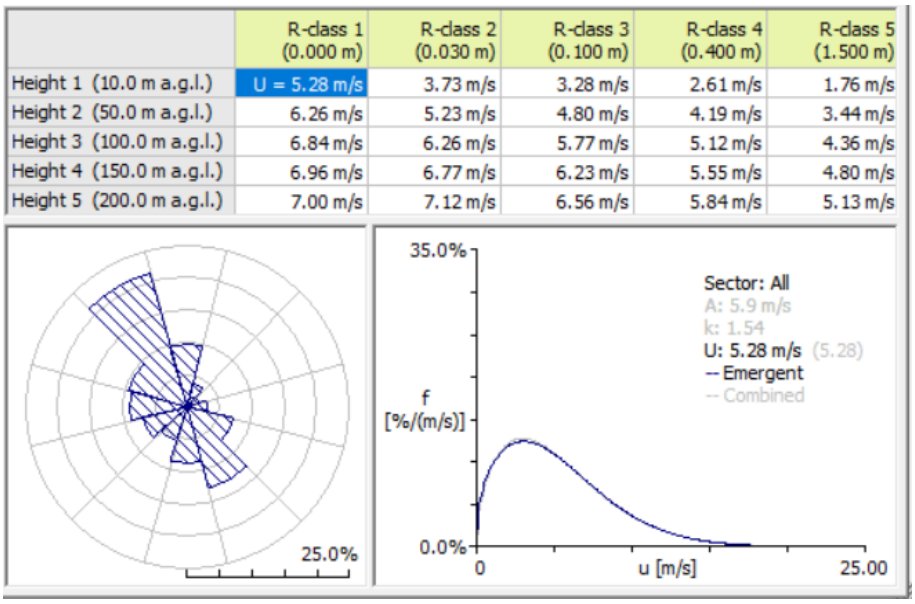

Figure 56: Wind rose and Weibull distribution for the site (from WAsP)

Each sector of the wind rose represents a wind direction (in 30° increments). The larger the blue wedge in a sector, the more frequently the wind blows from that direction throughout the year. On the right, the Weibull distribution is shown for all directions, indicating how frequently a particular wind speed occurs.

The values of interest for the presented case study are those in the row labeled “Height 4”, since the rotor of the IEA 15MW turbine is located at 150 meters above sea level.

Once the turbine specifications have been implemented, WAsP can generate the so-called Resource Grid, which allows the user to evaluate the turbine’s performance at every point on the site based on the previously identified wind characteristics. This is done using specific indicators such as the Annual Energy Production (AEP) or the Capacity Factor (CF)—the ratio between the AEP and the maximum extractable energy in one year.

WAsP calculates the AEP by simulating the wake using the Jensen model. The Resource Grid is displayed accordingly, showing—depending on the selected mode—values of wind speed, capacity factor, AEP, and power density.

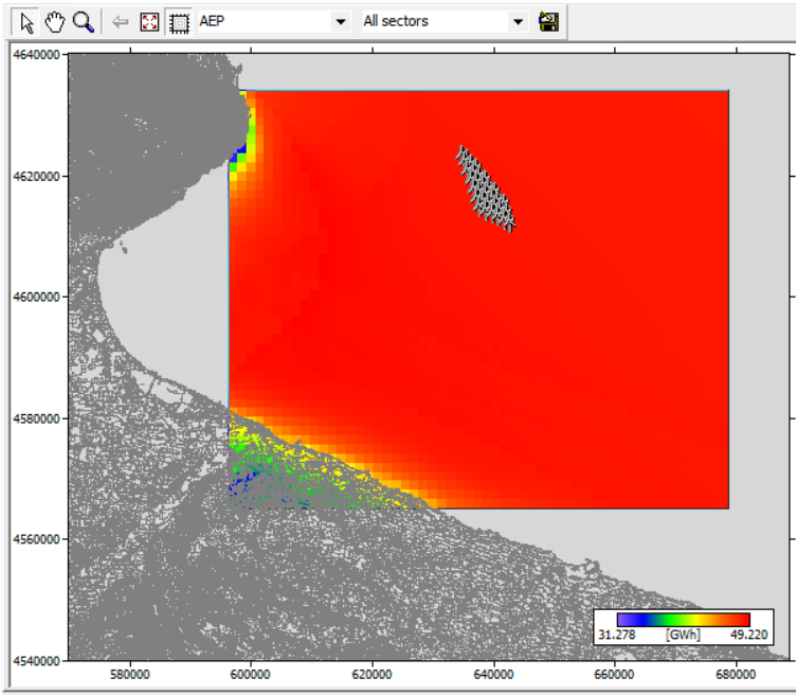

Figure 57: AEP variation in the site

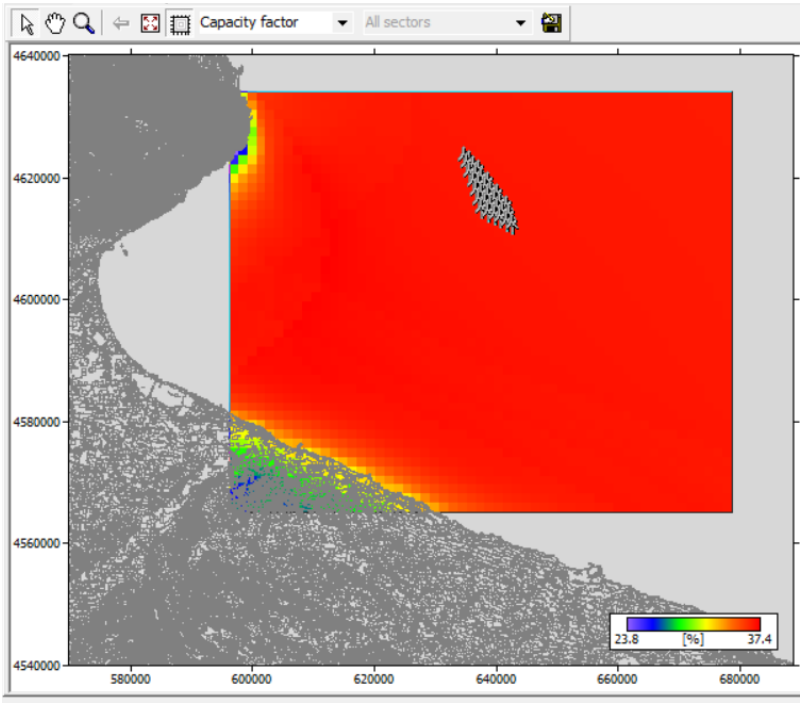

Figure 58: Capacity factor variation in the site

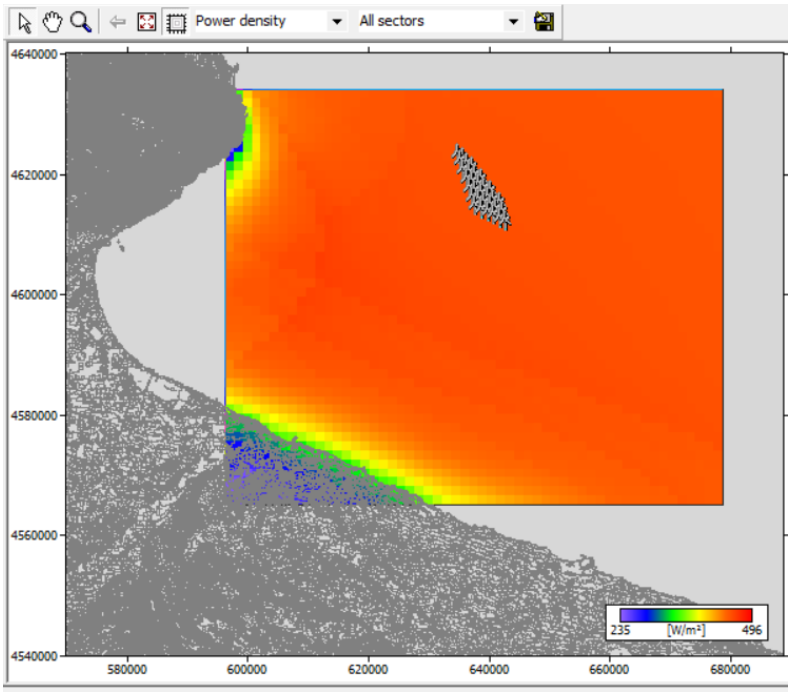

Figure 59: Power density variation in the site

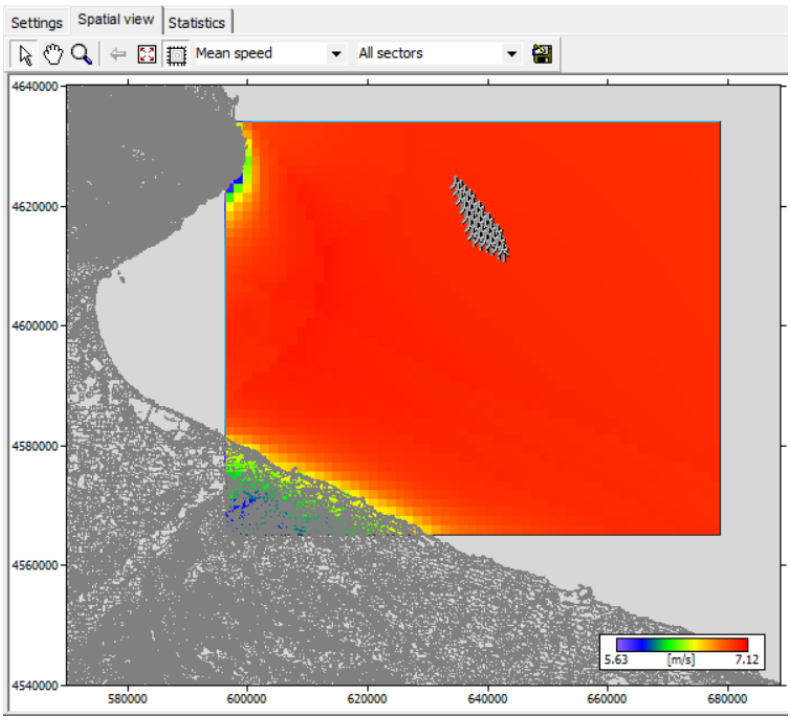

Figure 60: Mean speed variation in the site

Once the wind rose data is obtained, it can be implemented in PyWake in order to define the energy production within that environment as well. Site definition, in fact, requires setting the coefficients that fully characterize the Weibull

distribution—namely k, λ, and the frequency for each sector. The same applies to the definition of the turbine, which, in order to be used in PyWake, requires the power and thrust values for each wind speed in the scatter.

5.2. Wake Maps and Results

Once these elements are defined, the goal is to analyse the wake behaviour depending on the chosen model: the Jensen, Bastankhah, and Zong models were considered, keeping in mind that they offer varying degrees of accuracy in the near wake and far wake regions.

Table 2: Models setups

Name	Superposition Model	Wake Deficit Model	Deflection Model
Jensen 1983	SquaredSum	NOJ Deficit	JimenezWakeDeflection
Bastankhah PorteAgel 2014	WeightedSum	Bastankhah Gaussian Deficit	GCLHillDeflection
Zong PorteAgel 2020	LinearSum	Zong Gaussian Deficit	GCLHillDeflection

Common to all three models, the windfarm model *PropagateWind* and the rotor CGIRotorAvg models were selected, for the reasons previously discussed. The superposition models are selected for each wake deficit model as explained in Chapter 2. Deflection models are implemented in PyWake according to the type of wake model (top-hat or Gaussian). As for simulations conducted in FLORIS, the GCH and Cumulative Curl models were used.

Below are wake visualizations over satellite maps for each model and direction considered. A freestream wind speed of 15 m/s was consistently used, since higher values are less frequent according to the wind rose data. As for the wind directions, the ones blowing toward the coast (30°, 90°, and 120°) were selected, as they are more interesting in terms of potential land impacts, in addition to the 330° direction, which is the most frequent annually.

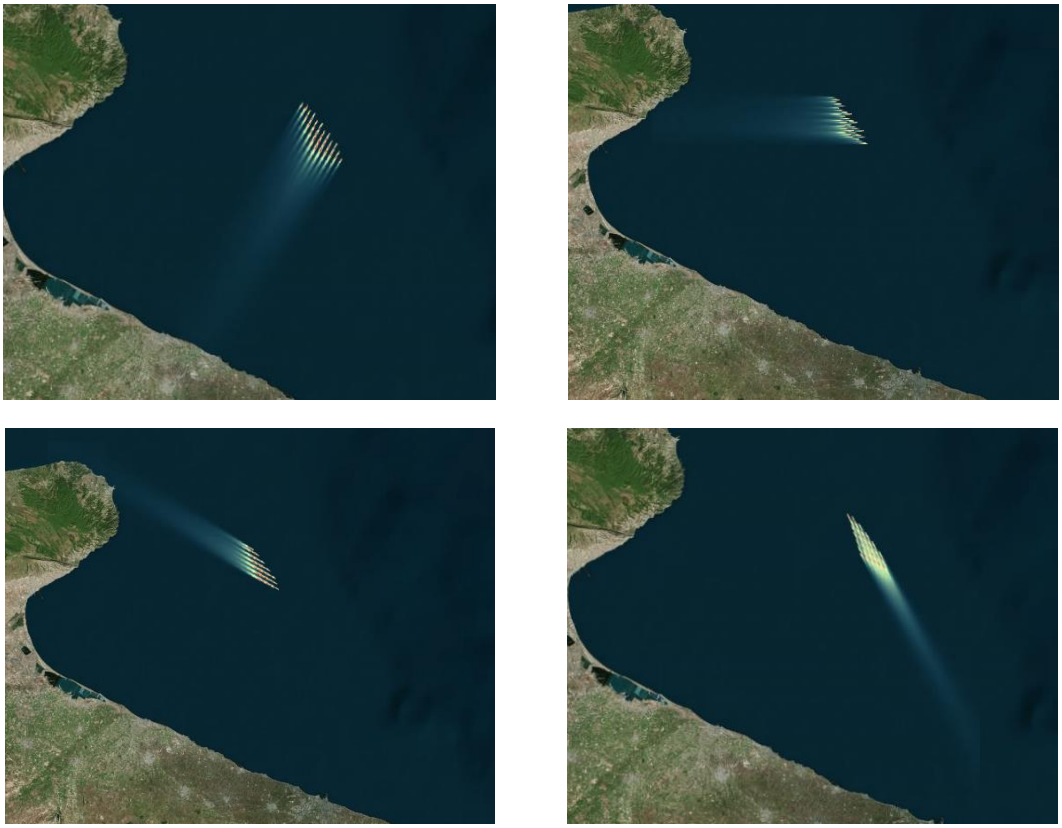

Figure 61: Georeferenced representations of wake map for wind directions of 30°, 90°, 120° and 330° for Bastankhah model

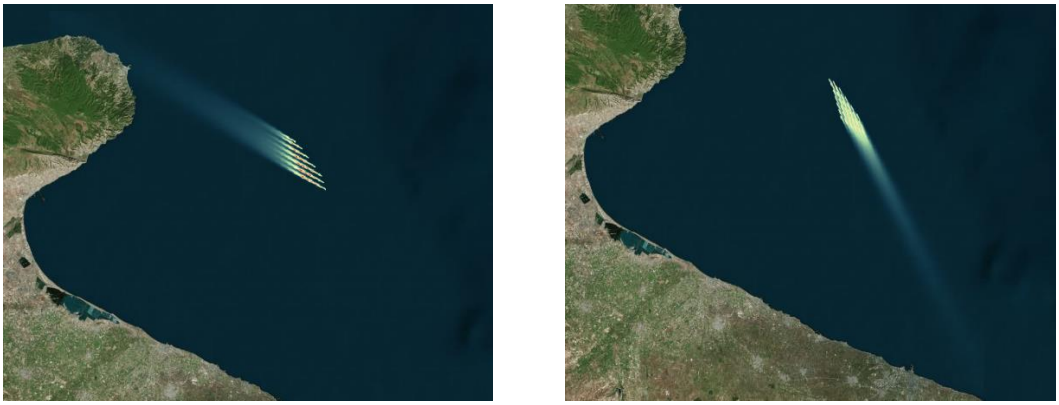

Figure 62: Georeferenced representations of wake map for wind directions of 30°, 90°, 120° and 330° for Zong model

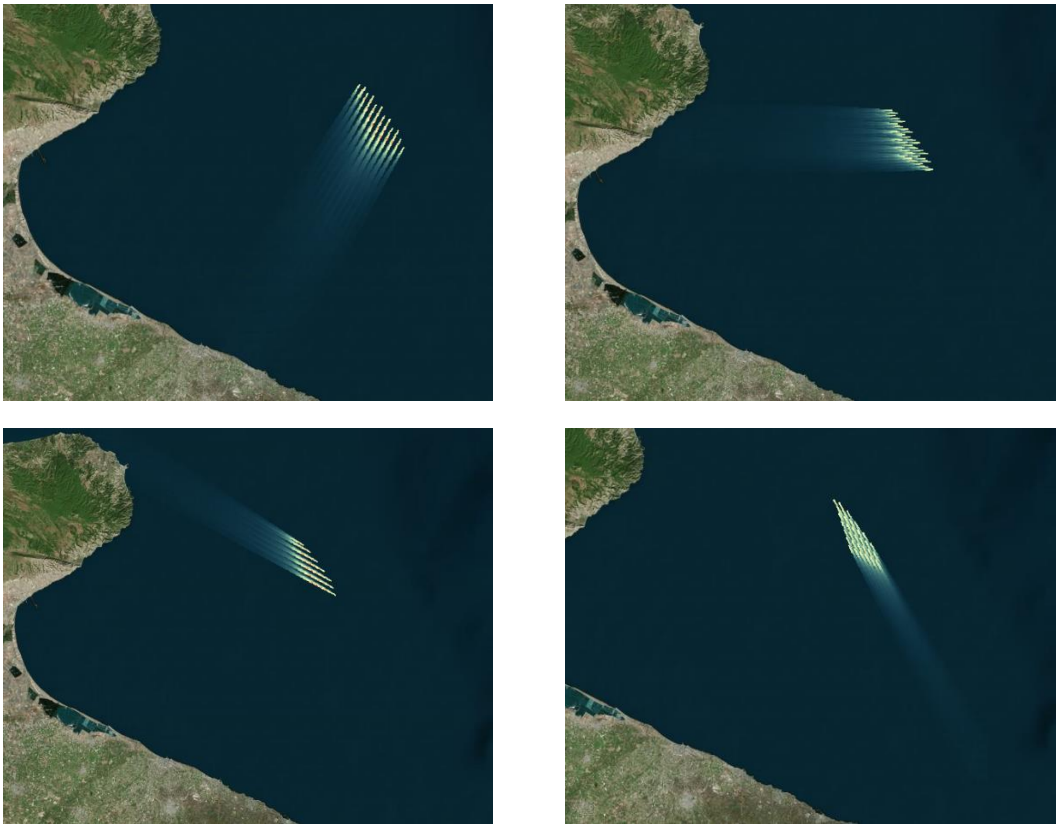

Figure 63: Georeferenced representations of wake map for wind directions of 30°, 90°, 120° and 330° for Jensen model

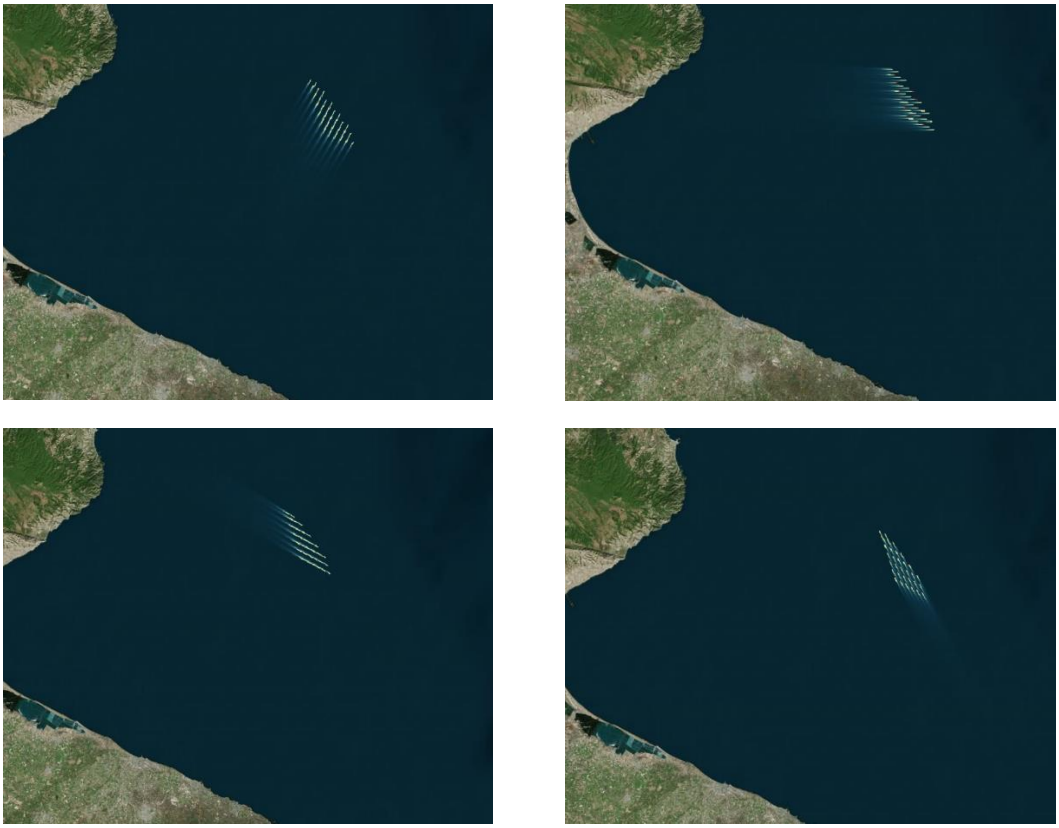

Figure 64: Georeferenced representation of wake map for wind directions of 30°, 90°, 120° and 330° for GCH model

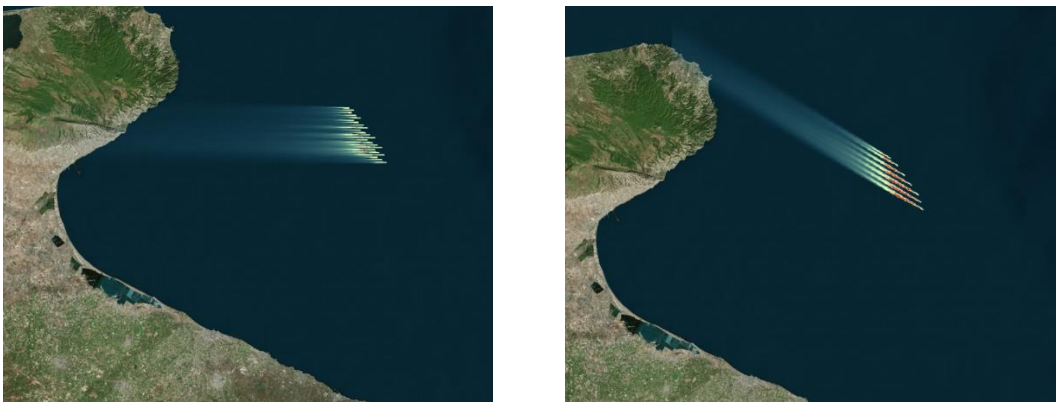

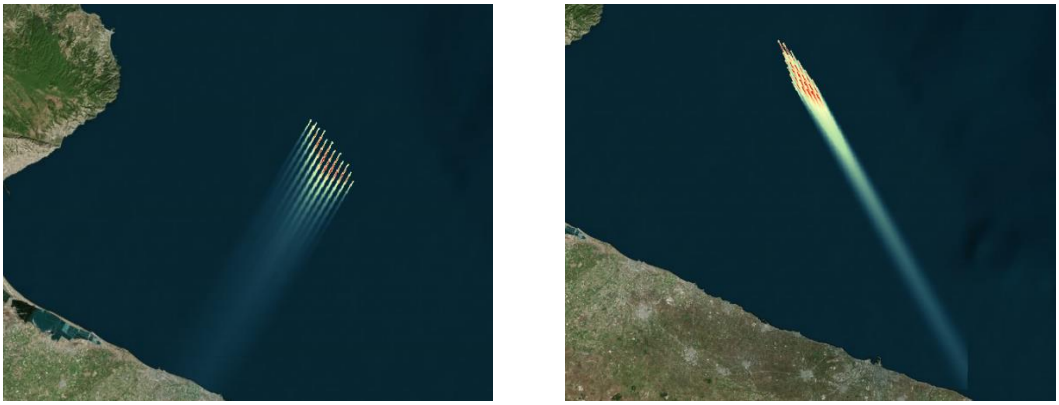

Figure 65: Georeferenced representation of wake map for wind directions of 30°, 90°, 120° and 330° for Cumulative Curl model

For the Cumulative Curl model, whose wake extends the furthest, the following observations can be made:

- At 30°, the wake extends over 50 km, reaching the coast.
- At 90° and 120°, the wake extends over 45 km, also reaching the coast.
- At 330°, the wake stretches over 60 km, brushing the coastline.

However, the wind speeds recorded along the coastline never fall below 14.8 m/s, resulting in a maximum deficit of less than 1.5%. According to [26], the threshold value considered significant for microclimatic impacts is 5%, so in this specific case—even in the worst-case scenarios—the wind recovers quickly enough to minimize the risk of impact.

The following table presents the wind speed recovery for each selected model:

Table 3: Speed recovery for each model

Model	Direction [°]	Speed recovery 95%: 14,25 m/s	Speed recovery 99%: 14,85 m/s
Common between FLORIS and PyWake			
Jensen	**30**	**~ 2,8 km**	**~ 33 km**
Jensen	**90**	**~ 1,7 km**	**~ 25 km**
Jensen	**120**	**~ 1,8 km**	**~ 24 km**
Jensen	**330**	**~ 3,3 km**	**~ 32 km**

PyWake			
Bastankhah	30	~ 3,4 km	~ 28 km
Bastankhah	90	~ 2,1 km	~ 20 km
Bastankhah	120	~ 1,9 km	~ 20 km
Bastankhah	330	~ 3,9 km	~ 32 km
Zong	30	~ 2,8 km	~ 24 km
Zong	90	~ 2,2 km	~ 18 km
Zong	120	~ 2 km	~ 16 km
Zong	330	~ 3,1 km	~ 27 km

FLORIS			
GCH	30	~ 1 km	~ 11 km
GCH	90	<1 km	~ 7 km
GCH	120	~ 1 km	~ 12 km
GCH	330	<1km	~ 9 km
Cumulative Curl	30	~ 4,7 km	~ 50 km
Cumulative Curl	90	~ 4,3 km	~ 45 km
Cumulative Curl	120	~ 4,1 km	~ 45 km
Cumulative Curl	330	~ 4 km	~ 60 km

It is evident how the default models in FLORIS differ significantly in terms of wake propagation: while the GCH model is quite conservative, limiting the deficits around the wind farm, the Cumulative Curl (CC) model, on the other hand, delays recovery much more, producing the most extended wake compared to the Bastankhah and Zong models implemented in PyWake. These latter two, though with some differences in terms of wind speed recovery, deliver more consistent results between each other than the models in FLORIS.

The Jensen model, which is available in both software tools, yields identical results in both. Although the model's theory suggests a more pronounced far wake compared to Gaussian models, the close spacing between turbines in this specific case study slows down the velocity recovery even in the Gaussian models, resulting in a far-wake effect similar to that of a top-hat model like Jensen.

5.3. Optimization strategy

We now aim to evaluate the wake effects in terms of productivity. In the previous chapter, an algorithm was developed to find the maximum AEP achievable through yaw control of the turbines in PyWake, allowing us to compare the results across

both the Zong and Bastankhah models, and potentially apply the methodology to all models available in the software.

The layout in PyWake is shown as follows:

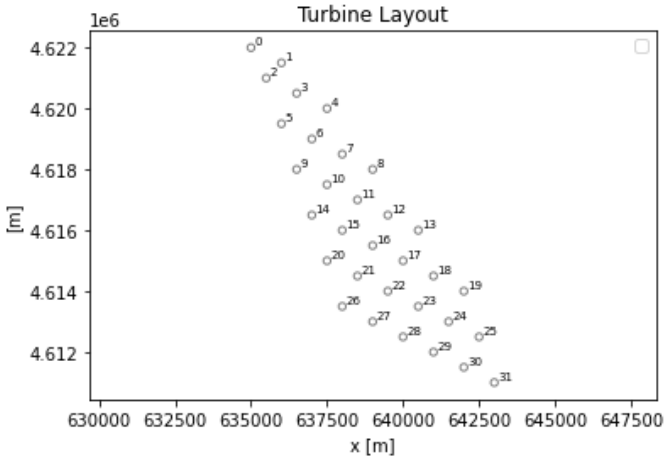

Figure 66: Wind farm layout shown in PyWake

The algorithm therefore derives, as seen in the base case, 12 different configurations, in each of which every turbine is oriented with the optimal angle found during the search. Beyond a certain wind speed, approximately 14 m/s, yaw optimization becomes ineffective, since high speeds tend to eliminate wake deflection, as discussed in Chapter 4. The maps shown below are the result of simulations carried out using the Bastankhah model, for a wind speed of 10 m/s and wind directions of 0°, 30°, 90°, and 120°:

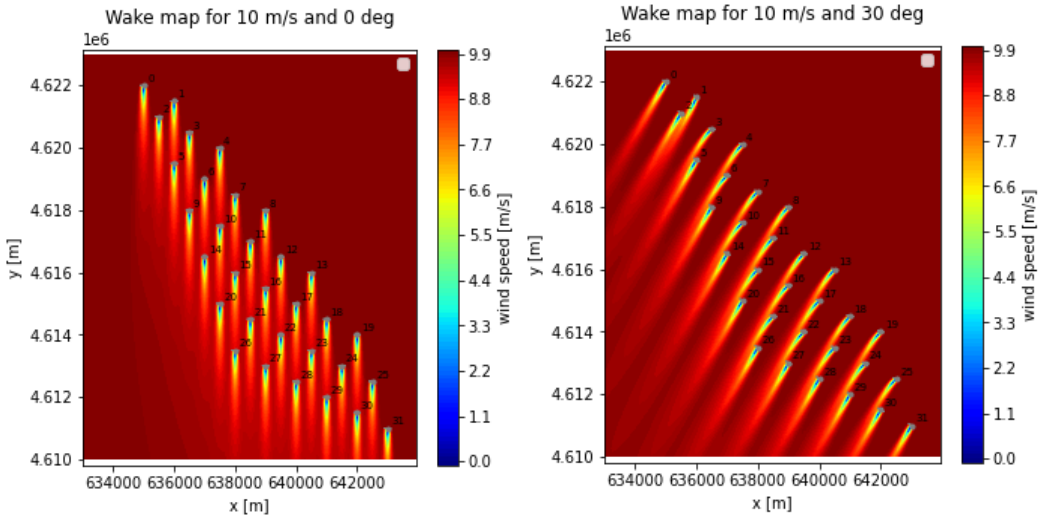

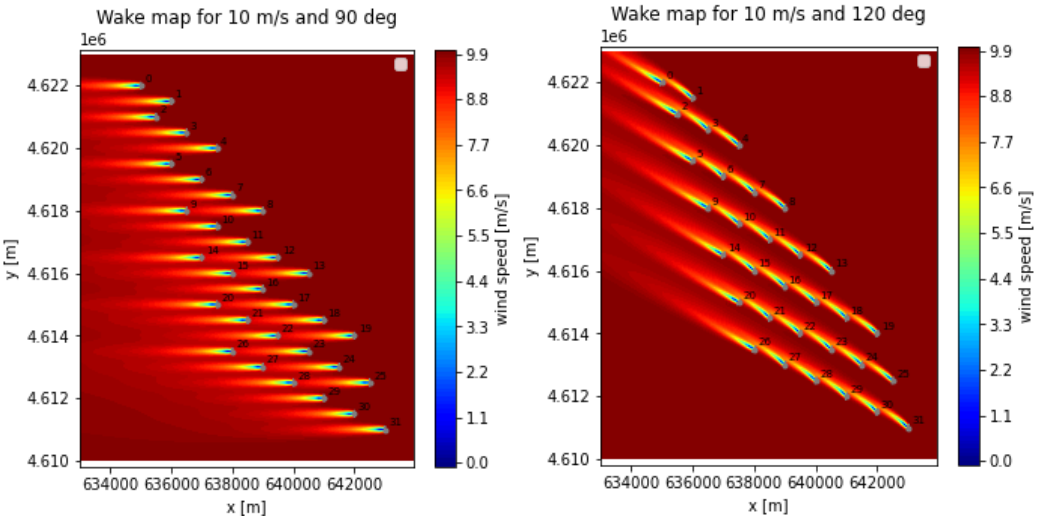

Figure 67: Wake map after yaw control strategy application for wind directions of 30°, 90°, 120° and 330°, for Bastankhah model

The effect of wake deflection is especially noticeable at 30° and 120°, while it is less significant or nearly absent at 0° and 90°. This is because wake deflection is more effective when many turbines are aligned with the wind direction: this is the case at 30°, where it is preferable for the turbines to generate deflected wakes that do not impact the downwind turbines. Conversely, at 0°, the yaw angles found have limited value, as the non-deflected wake is already sufficiently far from the downwind rotors. The effectiveness of the optimization depending on wind direction and speed is summarized in the following map, where the considerations just mentioned are illustrated:

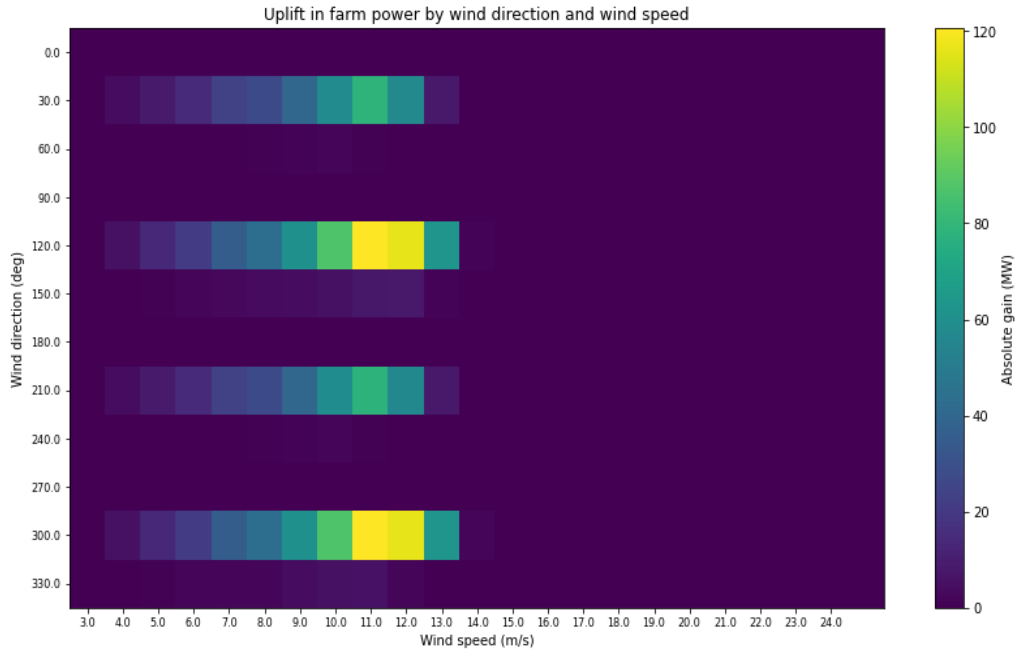

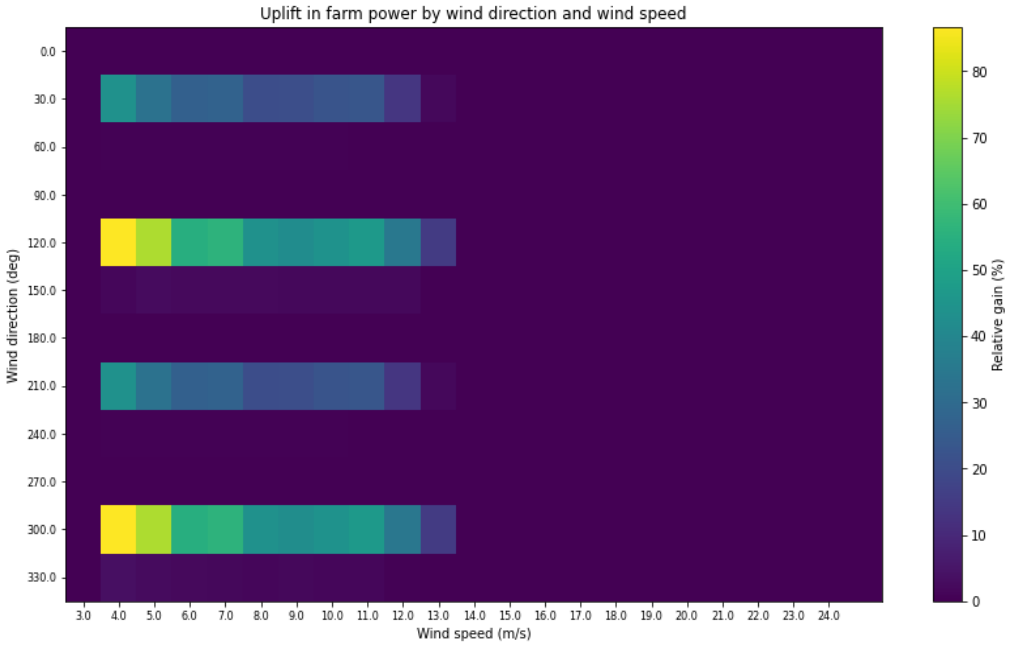

Figure 68: Absolute and relative gains in AEP for each wind speed and direction, for Bastankhah model

The absolute gain increases with wind speed, up to a cut-off at 13 m/s, reaching a maximum of +120 MW of extractable power when the wind blows along the ESE-WNW direction. The relative gain, on the other hand, is always more significant at low wind speeds, where the power curve shows lower extractable power values and therefore greater potential for improvement: for the same direction, at a wind speed of 4 m/s, the power shows a maximum improvement of +85% compared to the power output of the plant with yaw fixed at zero degrees. The AEP is then calculated both with and without yaw control, yielding the following result:

```
🔴 Baseline AEP  : 1331.75 GWh
✅ Optimized AEP : 1392.33 GWh
Gain in wind farm annual energy production : 4.55 %
```

Figure 69: Results from script

The same analysis was carried out under the same wind and speed conditions using the Zong model, producing the following results:

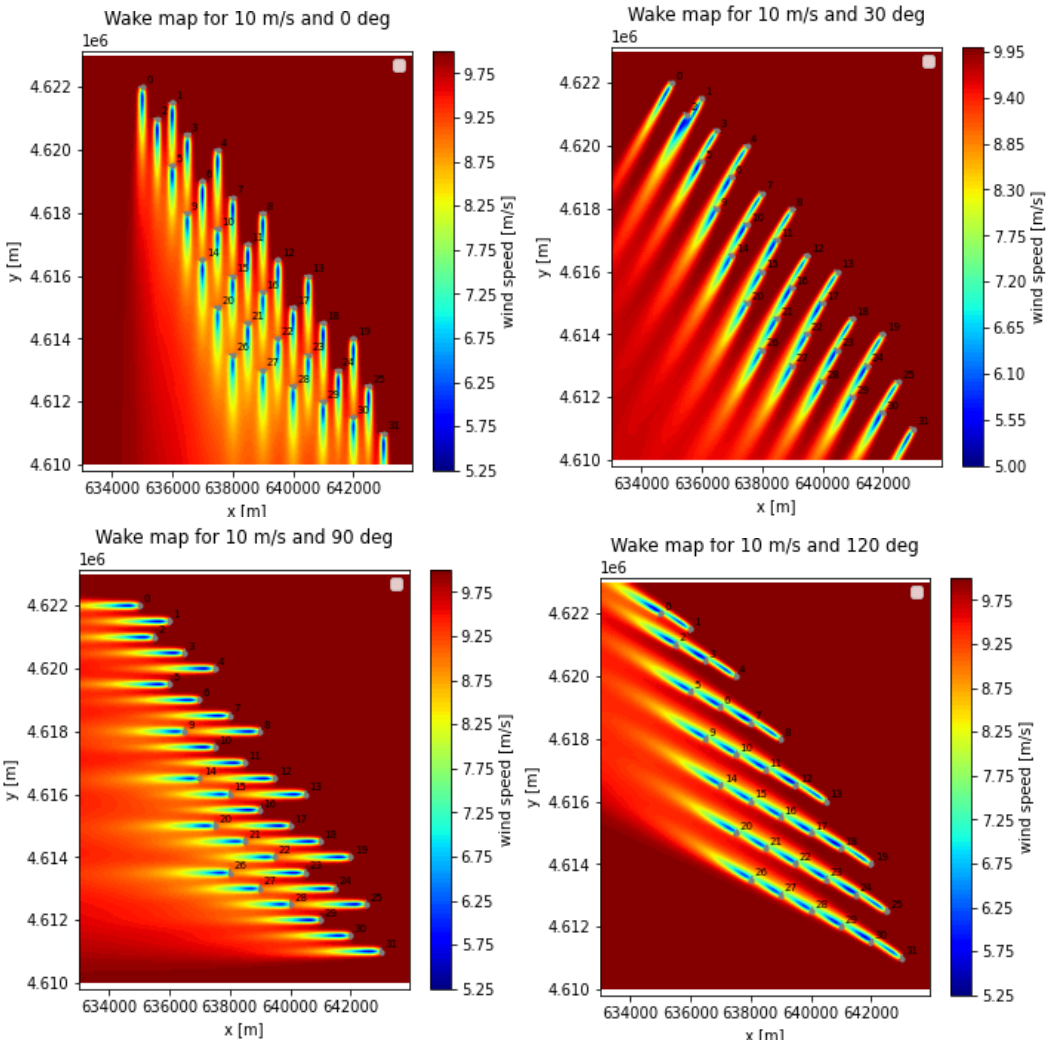

Figure 70: Wake map after yaw control strategy application for wind directions of 30°, 90°, 120° and 330°, for Zong model

Also in this case, for 0° and 90°, wake deflection is essentially absent, as the turbines are already arranged in a balanced manner to avoid downwind wake overlap. For 30° and 120°, however, the deflection is less pronounced compared to the previous case, with the algorithm detecting smaller values of optimal yaw angles. This is likely because the Zong model, unlike the Bastankhah model, models the far wake more accurately; therefore, excessive deflections could lead to increased turbulence for turbines positioned several rows downstream. In contrast, the Bastankhah model, which predicts significant velocity drops immediately behind the rotor, results in greater AEP values due to stronger deflections, allowing the downwind turbine to recover more wind speed.

The results by direction and speed using the Zong model are presented here.

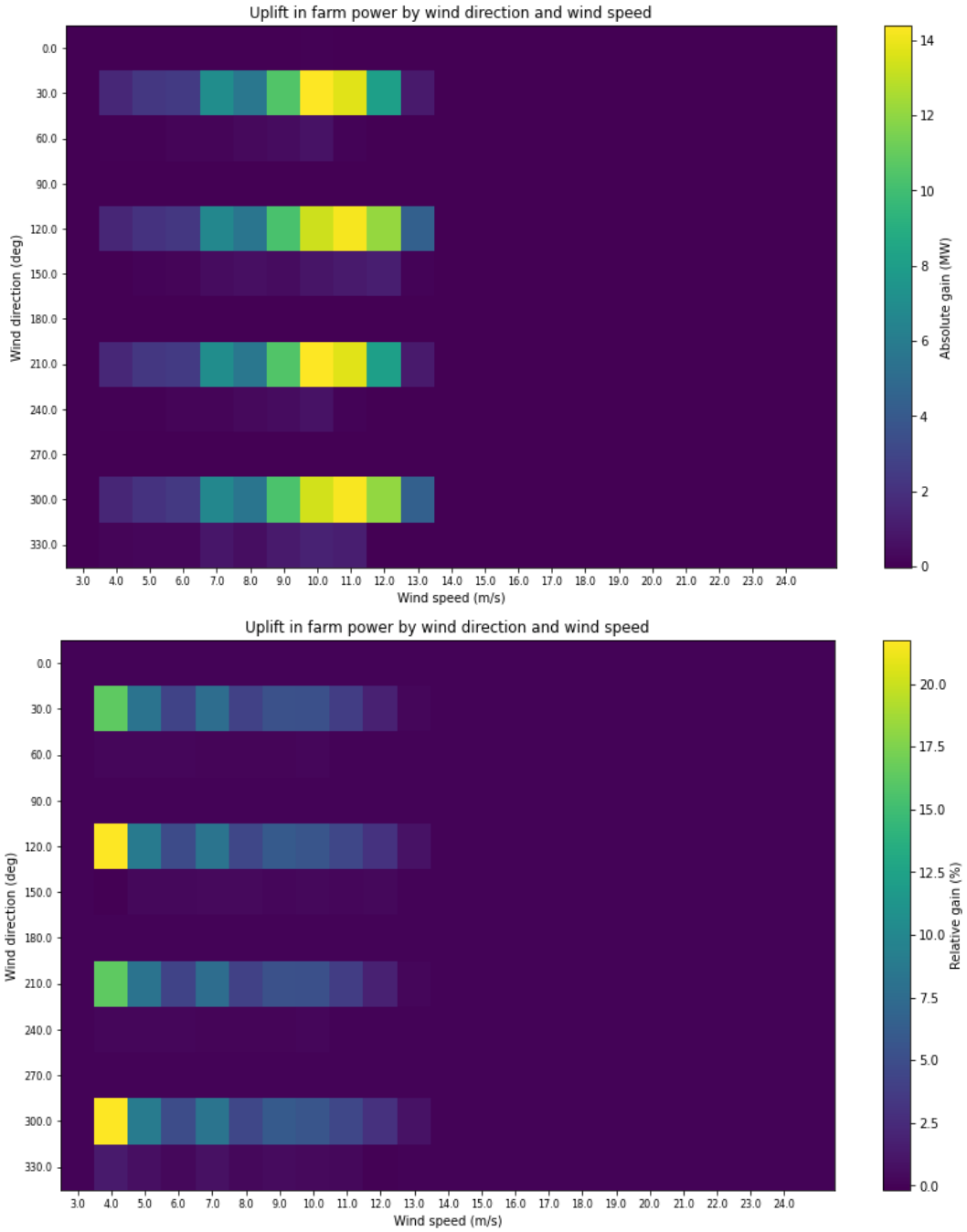

Figure 71: Absolute and relative gains in AEP for each wind speed and direction, for Zong model

In this simulation, very positive optimization results are also obtained for the NNE-SSW direction, although the absolute gain never exceeds +15 MW (at 10 m/s). The relative gain is also limited to a maximum of +20% at a wind speed of 4 m/s along the same direction, which is why we can expect the overall AEP increase to be lower:

```
Baseline AEP  : 1359.74 GWh
Optimized AEP : 1369.76 GWh
Gain in wind farm annual energy production : 0.74 %
```

Figure 72: Results from script

Finally, the Jensen model was analyzed in the same way:

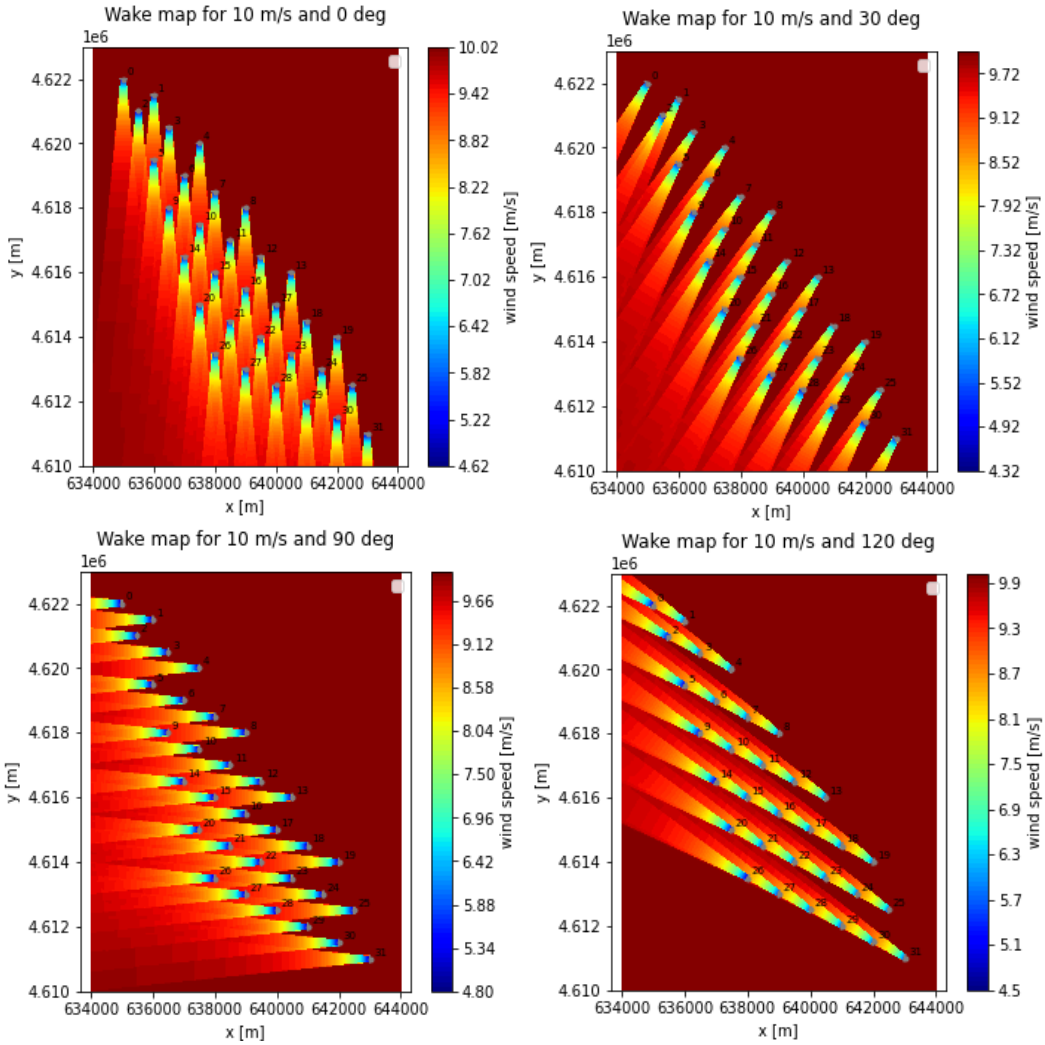

Figure 73: Wake map after yaw control strategy application for wind directions of 30°, 90°, 120° and 330°, for Jensen model

Here, as with the Zong model, the significance of the far wake results in limited and less noticeable deflection angles on the maps, though still present for wind directions of 30° and 120°. The results can be seen here:

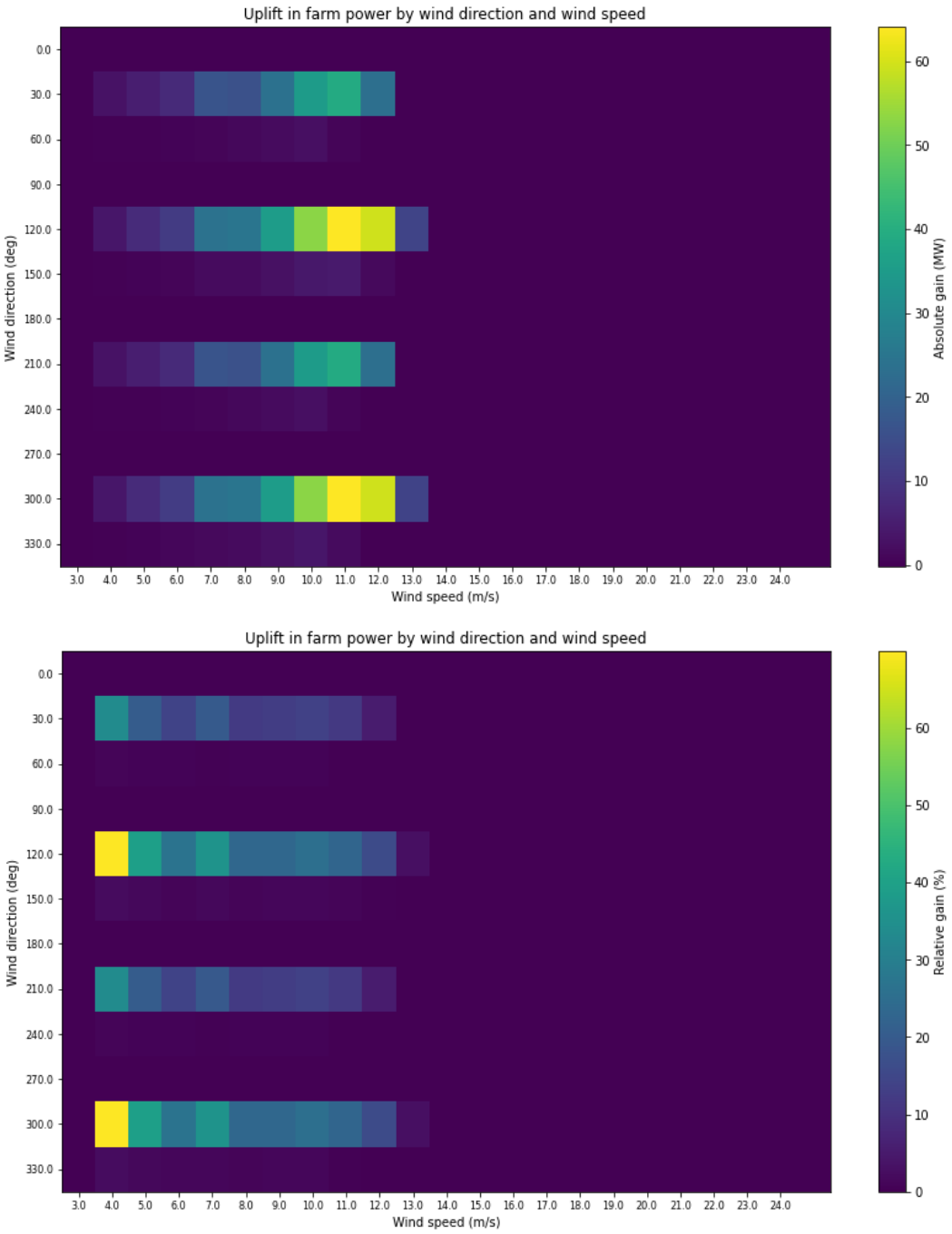

Figure 74: Absolute and relative gains in AEP for each wind speed and direction, for Jensen model

The direction with the most significant improvements remains ESE-WNW, with an absolute gain of +60 MW at 11 m/s, while the maximum relative gain is around +70%, again for wind speeds of 4 m/s. The AEP results are as follows:

```
🔴 Baseline AEP  : 1353.19 GWh
✅ Optimized AEP : 1387.45 GWh
Gain in wind farm annual energy production : 2.53 %
```

Figure 75: Results from script

Finally, each of these results is compared with a simulation run in FLORIS, using the GCH deficit/deflection model and the *YawOptimizerSR()* optimization method. The maps display the same wind directions used in the PyWake simulations:

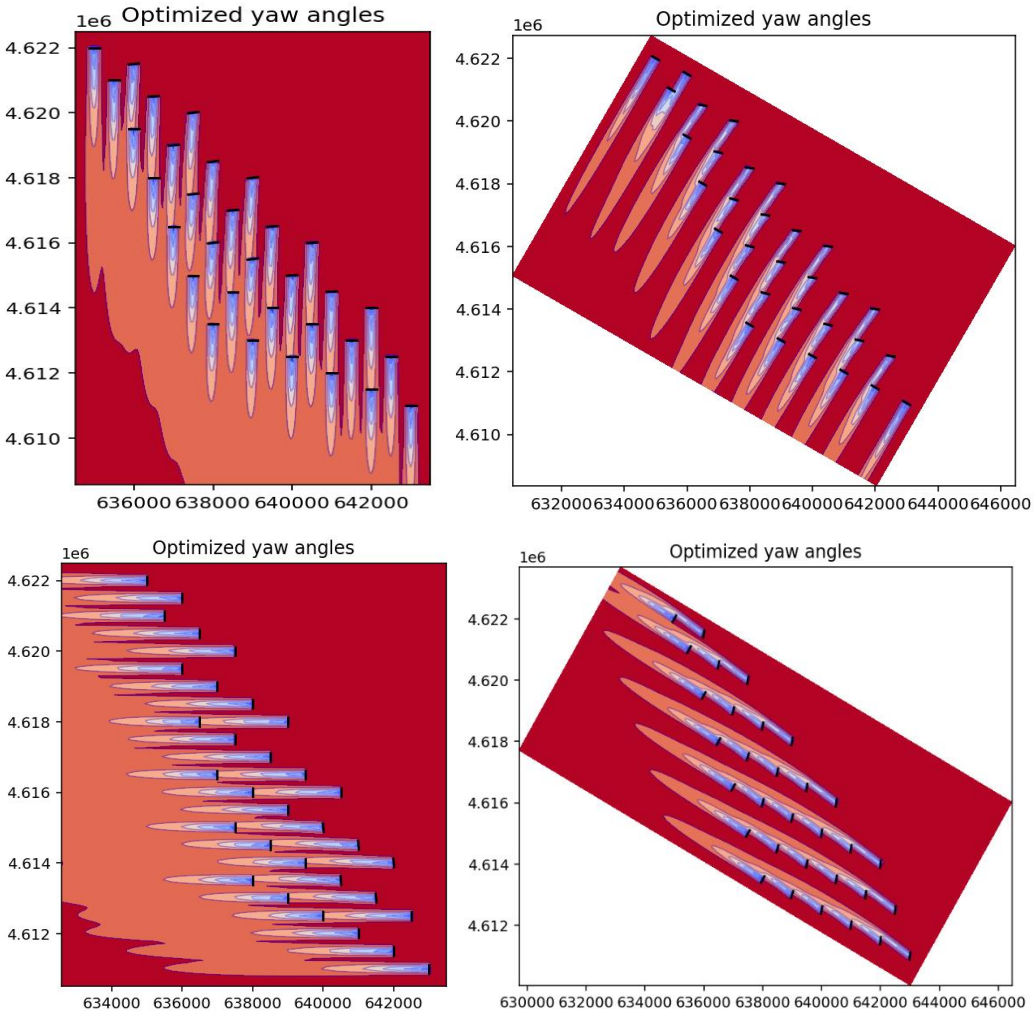

Figure 76: Wake map after yaw control strategy application for wind directions of 30°, 90°, 120° and 330°, for GCH model

As can be seen, the default algorithm in FLORIS generates yaw angles that reflect the behavior observed in the PyWake simulations, thereby confirming the reliability of the algorithm. The results for each wind direction-speed pair using GCH are consistent with those seen in the previous cases:

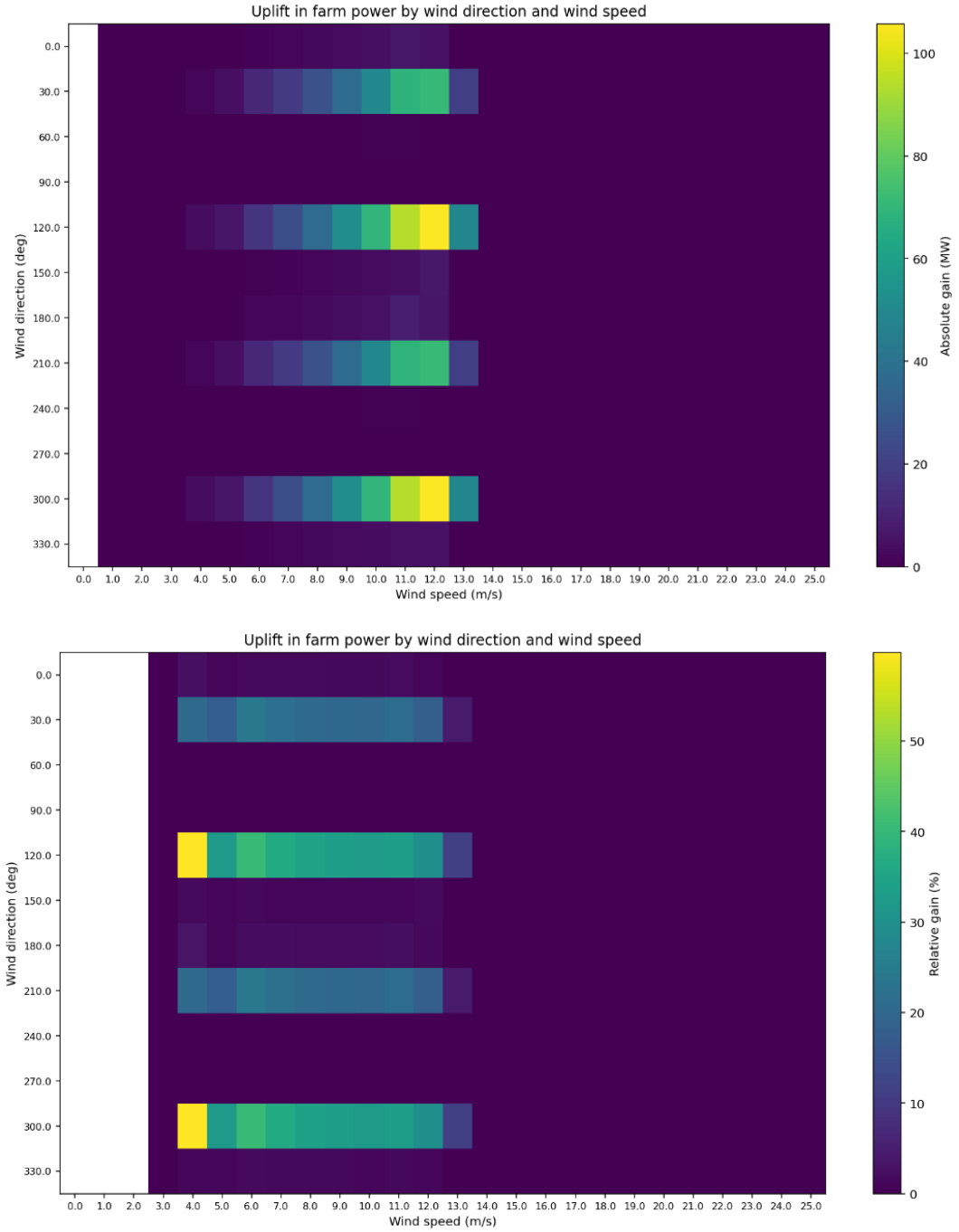

Figure 77: Absolute and relative gains in AEP for each wind speed and direction, for GCH model

In this last simulation, the maximum absolute gain exceeds 100 MW at wind speeds around 12 m/s for the ENE-WSW direction, while the maximum relative gain—again at 4 m/s—is approximately +60% in terms of total power output. The consequence of these high values in this chart is a significant increase in AEP under optimal yaw conditions:

```
Baseline AEP: 1331.87 GWh.
Optimal AEP: 1383.26 GWh.
Relative AEP uplift by wake steering: 3.858 %.
```

Figure 78: Results from script

5.4. Results comparison

We can now compare the different models and how they respond to yaw control:

Table 4: Comparison of results for each model

Model	Baseline AEP [GWh]	Optimized AEP [GWh]	AEP uplift [%]
Bastankhah	1331.75	1392.33	4.55
Zong	1359.74	1369.76	0.74
Jensen	1353.19	1387.45	2.53
GCH	1331.87	1383.26	3.86

It becomes clear that the choice of model can significantly impact the application of control and optimization strategies. In particular, the more a model emphasizes the mid-wake region, the more the algorithm is forced to limit yaw angles to prevent turbines located elsewhere in the wind farm from being hit by more turbulent winds. On the other hand, models that predict a rapid recovery of the wind speed deficit downwind and a lower wake expansion factor can make full use of the available yaw angle, significantly improving productivity.

6. Conclusions

Based on the analyses carried out, it can be generally concluded that a small-scale offshore wind farm located 50 km from the coast produces a wake with minimal long-range impact on the velocity field. The wind speed deficit—although it varies significantly depending on the model used—is negligible along the coastline in all simulations performed. Key factors that could alter this scenario include:

- The number of turbines and the layout of the wind farm, since a larger area occupied by turbines would lead to greater turbulence diffusion and, consequently, a more significant alteration in the mixing between the atmospheric boundary layer (ABL) and the overlying air masses.
- The turbine size, specifically the rotor diameter, as the swept area significantly influences wake generation. Therefore, the analyses presented here are particularly relevant for future scenarios involving increasingly larger turbines.

- The distance from the coast, since a shorter distance could result in more pronounced wind speed deficits reaching the shore, potentially influencing local precipitation patterns.
- The wind characteristics at the site, particularly the occurrences of specific wind speeds and directions. High wind speeds, if frequently coming from certain directions, could have a stronger impact. In this regard, most studies in the literature focus on North Sea sites, where wind behaviour is relatively homogeneous over large areas. The Mediterranean Sea, on the other hand, presents significant variability depending on geographic location, with some areas being much windier than others, or where one wind direction predominates. In the case study examined, high wind speeds are unlikely, so the wake impact remains, as mentioned, limited.

As for optimization, the results from both software tools confirm the effectiveness of the strategy. This is mainly because low-to-medium wind speeds are very frequent at the reference site, and these lower speeds yield the most benefit in terms of increased power output. However, the actual improvement must be assessed considering that the true wake behaviour cannot be predicted a priori based on the models selected in the analysis. It requires more in-depth investigation—such as with CFD tools, as discussed in Chapter 2—whereas models like PyWake and FLORIS can only simulate the wake behaviour theoretically.

Indeed, different models produce different outcomes: in the case of one specific model (Zong), optimization appears to have negligible effect, whereas for the other three models, yaw control yields positive results. This suggests that the wake behavior is such that optimization remains a viable strategy. Again, each analysis must be contextualized to the specific case: for instance, if the wind farm layout is not very tight, allowing faster downwind velocity recovery, or if the site is characterized by high wind speeds, yaw control would be less effective regardless of the assumed wake model.

References

[1] International Energy Agency, IEA. “Renewables 2024, Analysis and forecast to 2030” (2024). https://www.iea.org/reports/renewables-2024.

[2] WindEurope. “Wind energy in Europe 2024, Statistics and the outlook for 2025-2030” (2024). https://windeurope.org/intelligence-platform/product/wind-energy-in-europe-2024-statistics-and-the-outlook-for-2025-2030/

[3] Ministero dell’Ambiente e della Sicurezza Energetica. “Decreto 19 giugno 2024 recante “Incentivazione degli impianti a fonte rinnovabile innovativi o con costi di generazione elevati che presentino caratteristiche di innovazione e ridotto impatto sull’ambiente e sul territorio”” (2024). dm_19-06-2024_fer2-pdf.

[4] Meteorologische Zeitschrift Vol. 31 No. 4 (2022), p. 289 – 315. Schulz-Stellenfleth, Johannes; “Coastal impacts on offshore wind farms– a review focussing on the German Bight area”. 10.1127/metz/2022/1109

[5] Rajewski, D. A., E. S. Takle, J. H. Prueger,and R. K. Doorenbos (2016), “Toward understanding the physical link between turbines and microclimate impacts from *in situ* measurements in a large wind farm”, J. Geophys. Res. Atmos.,121, 13,392–13,414, doi:10.1002/2016JD025297

[6] S K Siedersleben *et a*l; Environ. Res. Lett. 13 124012; “Micrometeorological impacts of offshore wind farms as seen in observations and simulations” (2018). 10.1088/1748-9326/aaea0b

[7] Akhtar, Naveed; “Impacts of accelerating deployment of offshore windfarms on near-surface climate” (2022). https://www.nature.com/articles/s41598-022-22868-9

[8] DTU Wind Energy, “WAsP”. https://wasp.dtu.dk/

[9] DTU Wind Energy, “PyWake”. https://topfarm.pages.windenergy.dtu.dk/PyWake/

[10] NREL, “FLORIS”, https://nrel.github.io/floris/

[11] Sørensen, J. N. (2022). 2.07 – “Aerodynamic Analysis of Wind Turbines”. In T. M. Letcher (Ed.), Comprehensive Renewable Energy (2nd ed., Vol. 2, pp. 172-193). Elsevier. https://doi.org/10.1016/B978-0-12-819727-1.00127-8

[12] IMUK, “PALM”. https://palm.muk.uni-hannover.de/trac

[13] NREL, “WindSE”. https://www.nrel.gov/samples/other/software-module/windse-wind-systems-engineering

[14] Sorensen, J. N., and Shen, W. Z. (May 28, 2002). "Numerical Modeling of Wind Turbine Wakes ." ASME. *J. Fluids Eng*. June 2002; 124(2): 393–399. https://doi.org/10.1115/1.1471361

[15] NREL, “SOWFA”. https://www.nrel.gov/wind/nwtc/sowfa

[16] OpenCFD Ltd., “OpenFOAM”. https://www.openfoam.com/

[17] Jensen, N. O. (1983). “A note on wind generator interaction”. Risø National Laboratory. Risø-M No. 2411

[18] Majid Bastankhah, Fernando Porté-Agel, “A new analytical model for wind-turbine wakes” Renewable Energy, Volume 70 (2014), Pages 116-123, https://doi.org/10.1016/j.renene.2014.01.002

[19] Blondel, F.: Brief communication: “A momentum-conserving superposition method applied to the super-Gaussian wind turbine wake model”, Wind Energ. Sci., 8, 141–147, https://doi.org/10.5194/wes-8-141-2023 (2023)

[20] Shapiro, C. R., Starke, G. M., Meneveau, C., & Gayme, D. F. (2019). “A Wake Modeling Paradigm for Wind Farm Design and Control”. *Energies*, *12*(15), 2956. https://doi.org/10.3390/en12152956

[21] Scipy, “Scipy”. https://scipy.org

[22] Rathmann, O. S., Hansen, B. O., Hansen, K. S., Mortensen, N. G., & Murcia Leon, J. P. (2018). “The Park2 Wake Model - Documentation and Validation”. DTU Wind Energy E Vol. 160

[23] NREL. Gaertner, Evan; “Definition of the IEA 15-Megawatt Offshore Reference Wind”. Golden, CO: National Renewable Energy Laboratory. NREL/TP-5000-75698. https://www.nrel.gov/docs/fy20osti/75698.pdf

[24] DTU. “Global Wind Atlas”. https://globalwindatlas.info/en/about/introduction

[25] European Centre for Medium-Range Weather Forecasts, ECMWF, “ERA5”. https://cds.climate.copernicus.eu/datasets

[26] Platis, Andreas; “First *in situ* evidence of wakes in the far field behind offshore wind farms” (2018). https://www.nature.com/articles/s41598-018-20389-y